The Importance of Lake Littoral Zones for Estimating Arctic-Boreal Methane Emissions

Ethan D. Kyzivat[1], Laurence C. Smith[1], Fenix Garcia-Tigreros[2], Chang Huang[1, 3], Chao Wang[4], Theodore Langhorst[4], Jessica V. Fayne[5], Merritt E. Harlan[6], Yuta Ishitsuka[6], Dongmei Feng[6], Wayana Dolan[4], Lincoln H Pitcher[5, 8], Kimberly P. Wickland[7], Mark M. Dornblaser[7], Robert G. Striegl[7], Tamlin M. Pavelsky[4], David E. Butman[2,9], and Colin J. Gleason[6]

[1]Department of Earth, Environmental & Planetary Sciences and Institute at Brown for Environment & Society, Brown University, Providence, RI, 02912 USA

[2]School of Environmental and Forest Sciences, University of Washington, Seattle, WA, 98195 USA

[3]School of Urban and Environmental Sciences, Northwest University, Xi'an, Shaanxi, 710127 China

[4]Department of Earth, Marine and Environmental Sciences, University of North Carolina, Chapel Hill, NC, 27599 USA

[5]Department of Geography, University of California-Los Angeles, Los Angeles, CA, 90095 USA

[6]Department of Civil and Environmental Engineering, University of Massachusetts, Amherst, MA, 01003 USA

[7]Water Resources Mission Area, U.S. Geological Survey, Boulder, CO, 80303 USA

[8]Cooperative Institute for Research in Environmental Sciences (CIRES). University of Colorado, Boulder. Boulder, CO, 80309, USA.

[9]School of Engineering and Environmental Sciences, University of Washington, Seattle, WA, 98195 US

Corresponding author: Ethan D. Kyzivat (ethan.kyzivat@aya.yale.edu)

Key Points:

- We provide a first quantification of vegetated littoral zone areas across 4,572 lakes in four Northern study areas using airborne mapping.
- Vegetated lake littoral zones vary regionally from 1 to 59 percent of lake area, and also vary seasonally to a lesser degree.
- Accounting for these zones leads to a 79 percent increase in methane upscaling estimates.

Abstract

Shallow areas of lakes, known as littoral zones, emit disproportionately more methane than open water but are typically ignored in upscaled estimates of lake greenhouse gas emissions. Littoral zone coverage may be estimated through synthetic aperture radar (SAR) mapping of emergent aquatic vegetation, which only grows in water less than ~1.5 m deep. To assess the importance of littoral zones to landscape-scale methane emissions, we combine airborne SAR mapping with field measurements of littoral and open-water methane flux. First, we use Uninhabited Aerial Vehicle SAR (UAVSAR) data from the NASA Arctic-Boreal Vulnerability Experiment (ABoVE) to map littoral zones of 4,572 lakes across four Arctic-boreal study areas and find they comprise ~16% of lake area on average, exceeding previous estimates, and exhibiting strong regional differences (averaging 59 [50–68]%, 22 [20-25]%, 1.0 [0.8-1.2]%, and 7.0 [5.0-12]% for the Peace-Athabasca Delta, Yukon Flats, and northern and southern Canadian Shield areas, respectively). Next, we account for these vegetated areas through a simple upscaling exercise using representative, paired open water and littoral methane fluxes. We find that inclusion of littoral zones nearly doubles overall lake methane emissions, with an increase of 79 [68 – 94]% relative to estimates that do not differentiate lake zones. While littoral areas are proportionately greater in small lakes, this relationship is weak and varies regionally, underscoring the need for direct remote sensing measurements using vegetation or otherwise. Finally, Arctic-boreal lake methane upscaling estimates can be improved by more measurements from both littoral zones and pelagic open water.

Plain Language Summary

Lakes are one of the largest natural sources of the greenhouse gas methane and are especially common in high latitudes. The shallow, near-shore areas of lakes, known as littoral zones, emit disproportionately more methane than open water areas, but are typically ignored in broad-scale estimates of lake greenhouse gas emissions. While lake depths are difficult to map from airborne imagery, littoral zone coverage can be approximated by mapping emergent aquatic vegetation, which only grows in water less than ~ 1.5 m deep, and are detectable via radar remote sensors. To assess the importance of littoral zones to landscape-scale methane emissions, we combine airborne radar mapping with field measurements of littoral and open-water methane emissions. Littoral zones vary regionally and comprise ~16% of lake area on average, a greater amount than previous estimates. A simple estimate using paired open water and littoral methane emission values shows inclusion of littoral zones nearly doubles overall lake methane emissions estimates. Littoral zone coverage has little relationship with lake size, making it hard to predict. Therefore, to better estimate methane emissions, we suggest using remote sensing to inform littoral zone maps and collecting methane emission measurements from both littoral zones and lake centers.

1 Introduction

Inland waters are the single largest natural source of the greenhouse gas methane (CH_4) (Saunois et al., 2020; Wik, et al., 2016). Lakes are estimated to be responsible for ~24% of all inland water emissions, second only to wetlands (Bastviken, Tranvik, Downing, Crill, & Enrich-Prast, 2011; Saunois et al., 2020). They emit methane via diverse pathways of diffusion, ebullition, transport through aquatic plant tissue, and through a storage flux during turnover in stratified lakes. Emissions are strongly dependent on temperature, sediment carbon content, redox environment, and gas transfer velocity (Bastviken, Cole, Pace, & Tranvik, 2004; Wik et al., 2016). Uncertainties in upscaling lake emissions therefore have vast spatial and temporal heterogeneities (Loken et al., 2019; Natchimuthu et al., 2016; Stephanie et al., 2020).

Lake emission upscaling efforts have only recently begun to account for lake surface area (DelSontro et al., 2016; Hastie et al., 2018; Holgerson & Raymond, 2016), but it is still rare to consider other aspects of morphometry, such as slope and littoral area (Casas-Ruiz et al., 2021). "Bottom-up," or process-based, methane models tend to over-predict methane fluxes compared to "top-down," or inversion-based, models, and double-counting of small lakes as wetlands caused by mismatch in scale and methods among datasets has been suggested as a possible cause (Thornton, Wik, & Crill, 2016). Small (< 0.001 km^2) lakes and wetlands are poorly mapped, especially in Arctic-boreal regions containing the world's greatest abundance of lakes (Verpoorter et al., 2014). Indeed, uncertainty in wetland extent is frequently cited as the leading cause of uncertainty in bottom-up methane estimates (Zhang et al. 2017), and errors arising from large-scale extrapolations of heterogeneous wetlands have also been noted (Bridgham et al., 2013).

As the most "wetland-like" zone within lakes, littoral zones are important sources of carbon and known methane emission hot spots (Bergström et al., 2007; Burger et al., 2016; Huttunen et al., 2003; Juutinen et al., 2003; Larmola et al., 2004; Natchimuthu et al., 2016). The littoral zone is the area in or near a lake or pond lying between the outer edge of the eulittoral zone (inundated for only part of the year), to the maximum depth supporting submerged macrophyte (aquatic vegetation) growth, i.e., the deepest water where light can penetrate the entire water column (but no greater than ~10 m for vascular angiosperms; Wetzel, 2001). Emergent macrophytes can only grow in water < ~1.5 m deep, denoted the upper littoral zone (Wetzel, 2001). These plants can act as conduits to the atmosphere for methane produced in lake sediments (Dacey and Klug, 1979; Colmer, 2003). They also produce carbon compounds that are preferentially consumed by methanogens (methane-producing bacteria), and their decomposing biomass and root exudates are a large contributor to sediment organic carbon (Christensen et al., 2003; Joabsson, Christensen, & Wallén, 1999; Ström, Mastepanov, & Christensen, 2005). Previous studies have noted the tendency for small (Michmerhuizen, Striegl, & McDonald, 1996; Bastviken et al., 2004; Holgerson & Raymond, 2016; Engram et al. 2020) and shallow (West et al., 2015; Wik et al., 2016; Li et al., 2020) lakes to emit more methane than larger and deeper ones. Within a single lake, depth often prohibits methane ebullition due to water overburden pressure (Bastviken et al., 2004), although there are exceptions (Huttunen et al., 2003). Deeper waters also provide more opportunity for microbe-mediated oxidation of dissolved methane (DelSontro et al., 2016). Emergent aquatic plants may thus be used as a proxy for shallow (up to ~1.5 m), carbon-rich, methanogenic lake sediments with less opportunity for oxidation of methane in the overlying water column.

Plant-based emissions are measured least frequently of all lake pathways (Bastviken et al., 2011; Wik et al., 2016), along with open-water emissions near plants, so methane upscaling estimates in lakes (DelSontro, Beaulieu, & Downing, 2018; Tranvik et al., 2009) usually rely solely on pelagic open water fluxes. Yet fluxes measured from vegetated regions can be statistically greater than those from open water (Villa et al., 2021), often contributing the majority of whole-lake emissions, with estimates derived from open water measurements shown to underestimate total flux by 5-78% (Natchimuthu et al., 2016). Plant-based fluxes can be significant at the landscape scale, for example exceeding peatland emissions in southern Finland by 30%, despite covering only 40% as much area (Bergström et al., 2007). Another study of three Finnish lakes found that the vegetated littoral zone produced 66-77% of whole-lake emissions (Juutinen et al., 2003). Emergent macrophytes are estimated to emit 11% of the equivalent from all open water lakes, rivers, and reservoirs combined globally (Bastviken et al., 2011). For these reasons, more methane flux measurements in lake littoral zones and estimates of total macrophyte coverage are needed (Bergström et al., 2007; Schmiedeskamp et al., 2021).

However, vegetated littoral coverage is poorly constrained. Duarte et al. (1986) suggested that emergent macrophytes colonize on average 7% of a lake regardless of its area, while submerged macrophyte coverage generally declines with area. They list light availability, sediment characteristics, and trophic status as key characteristics for macrophyte growth, with slope as the greatest predictor of emergent macrophyte coverage. Others have theorized that the percent of a lake's surface area covered with macrophytes scales with nitrogen concentration and the inverse of mean depth (Smith and Wallsten 1986), or scales inversely with lake area (Michmerhuizen et al., 1996) or perimeter (Bergström et al., 2007). Mäkelä et al. (2004) similarly found that an average of 6% (range: 1-100%) of total lake area was covered by macrophytes in a sample of 50 lakes and that total fractional macrophyte coverage per lake steeply declined with lake area. Zhang et al. (2017) compiled a synthesis database of aquatic macrophytes in 155 global lakes and observed an average coverage of 26% (range: 0.000-100%) with an accelerating decline since 1900.

Remote sensing studies have used both optical and synthetic aperture radar (SAR) sensors to map macrophytes in lakes. Optical satellites are better suited to detecting vegetation type, while SAR can detect water even through vegetation canopies (Hess, Melack, & Simonett, 1990). Ghirardi et al. (2019) used optical Sentinel-2 satellite data to map submerged aquatic macrophytes in an Italian lake and noted both inter- and intra-annual variations in aerial coverage. Nelson et al. (2006) used Landsat Thematic Mapper imagery to map various types of macrophytes in 13 lakes in Michigan and found total macrophyte coverage ranging from 5-42%. Zhang et al. (2018) used TerraSAR-X SAR imagery to map macrophytes in nine Brazilian reservoirs and similarly found large spatial and temporal variation in coverage. Thus, many remote sensing studies have demonstrated spatial and/or temporal differences in aquatic macrophyte cover, yet few have measured total coverage across large geographical areas and numerous lakes. Littoral zone area statistics, therefore, remain confined to a handful of studies of small numbers of lakes.

Here, we aim to quantify the fractional coverage of emergent macrophytes for thousands of lakes across four Arctic-boreal regions in order to assess lake littoral zone extents and their potential importance in scaling methane emissions. To estimate littoral zone extent, we use the canopy-penetrating properties of L-band synthetic aperture radar (SAR) flown during the NASA Arctic-Boreal Vulnerability Experiment (ABoVE) airborne campaign (2017-2019) to map emergent macrophyte coverage, a proxy for littoral zone extent. Next, we compile paired measurements of methane flux from open water and vegetated littoral zones. Finally, we use these flux measurements and our remote sensing-derived ranges in vegetated littoral coverage to estimate the sensitivity of lake methane emissions to littoral zone coverage. We conclude with discussion of the causes of regional differences, some broader recommendations for landscape-scale methane upscaling, study limitations, and recommendations for future research.

2 Study areas, data sources, and methods

2.1 Study areas

The NASA Arctic-Boreal Vulnerability Experiment (ABoVE) campaign is a decade-long effort to measure environmental change in the Arctic and boreal regions of western North America via coordinated ground measurements and airborne remote sensing (Miller et al., 2019). Here, we focus on four study areas within the ABoVE domain, each corresponding to one or more flight lines from its airborne campaigns:

1) Peace-Athabasca Delta, Alberta, Canada (PAD);
2) Southern Canadian Shield near Baker Creek (CSB), Northwest Territories, Canada;
3) Interior Canadian Shield near Daring Lake (CSD), Northwest Territories, Canada; and
4) Yukon Flats National Wildlife Refuge, Alaska, USA (YF).

These four study areas were chosen because of their high lake density and contrasting geological, hydrological, and ecological conditions. The PAD is one of the world's largest inland deltas and is located on the western edge of Lake Athabasca (**Figure 1**). The overall relief of its lowland regions is 11 m, causing numerous marsh-type wetlands, mudflats, and lakes, many of which are recharged by the Athabasca River (Pavelsky & Smith, 2008), and more rarely, by ice-jam floods in the Peace River (Timoney, 2013). These floods can inundate up to 80% of the 5,600 km^2 delta (Töyrä & Pietroniro, 2005; Wolfe et al., 2006), while in typical years, 26% is covered by intermittently-inundated wetlands (Ward & Gorelick 2018). It is a Ramsar Wetland, UNESCO World Heritage site, and home to numerous endemic species of birds, fish, and mammals including the endangered whooping crane and the largest remaining herd of wood bison (Parks Canada, 2019). The two Northwest Territories study areas (CSD, CSB) are located on the Canadian Shield, the world's largest deposit of Precambrian-age bedrock and source of the oldest known terrestrial rocks (Slaymaker, 2016). Deglaciated only nine thousand years ago and with a rocky, sparse surface drainage pattern, the Shield is also the world's most lake-rich region and contains many peatlands (Slaymaker, 2016; Spence & Woo, 2006). CSB is underlain by discontinuous permafrost, while CSD crosses the tree line and contains a transition to continuous permafrost and the tundra/taiga ecotone (**Figure 1**). The YF is underlain by discontinuous permafrost in alluvial soils and contains lakes of various hydrologic connectivity to the Yukon River and its tributaries (Anderson et al. 2013, Johnston et al., 2020). Like the PAD, the YF has flat topography, permitting seasonal flooding during the early summer to cover large areas, and it is a source of both lateral riverine and water-air carbon fluxes (Striegl, et al., 2012). All four study areas are home to multiple indigenous and First Nation communities, as well as the city of Yellowknife and numerous smaller settlements.

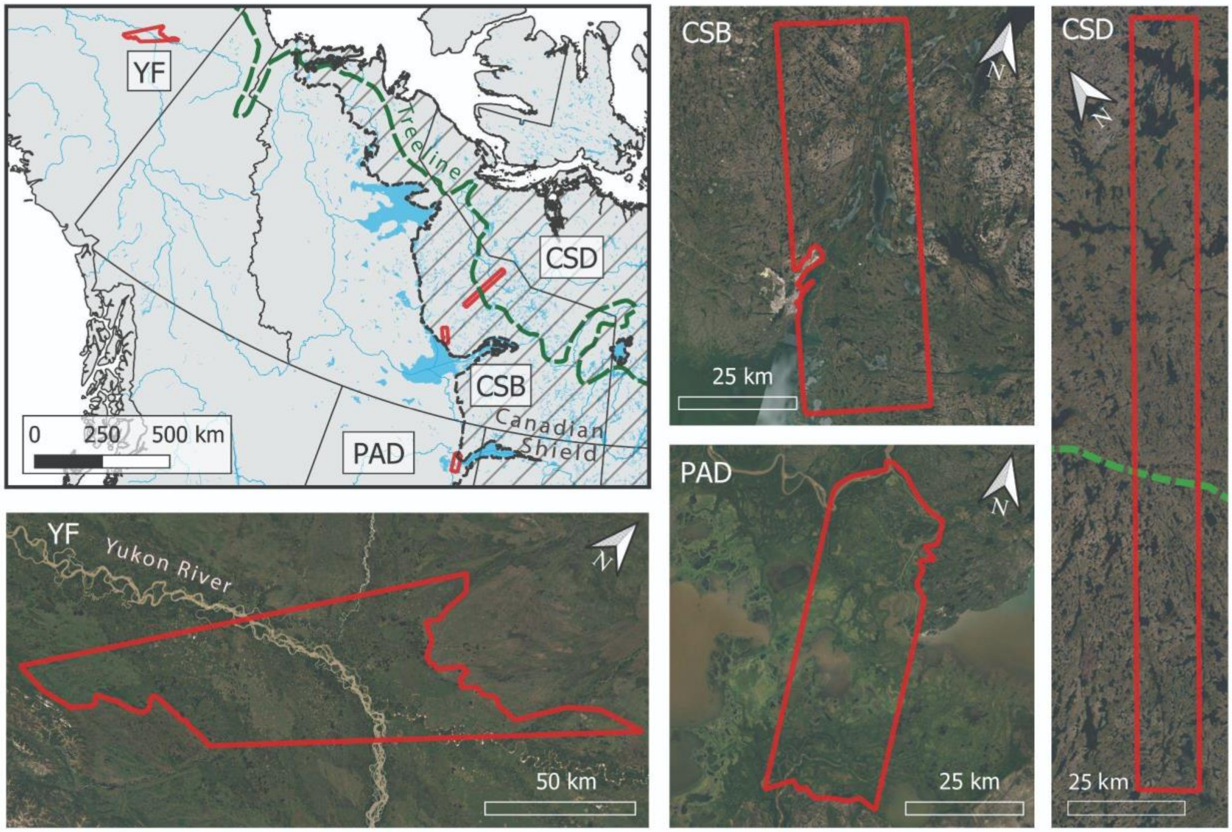

Figure 1. Location map of study areas (YF = Yukon Flats; CSD = Canadian Shield, Daring Lake; CSB = Canadian Shield, Baker Creek; PAD = Peace-Athabasca Delta). Study area boundaries (red polygons) are derived from intersecting UAVSAR airborne flight coverage with physiographic boundaries. Major water bodies are shown in blue; Canadian Shield with stippling, and the northern tree line limit (Brown et al., 2002) in green.

2.2 Data sources

2.2.1 Airborne polarimetric SAR

L-band synthetic aperture radar (SAR) data from the Uninhabited Aerial Vehicle Synthetic Aperture Radar (UAVSAR) were obtained in multi-look ground-projected format (GRD) and reprojected to ~5.5 m spatial resolution (NASA/JPL 2017-2019) on the ABoVE Science Cloud computing environment. With a wavelength of 23.8 cm, UAVSAR has been used extensively for vegetation mapping and inundation detection, including in lowlands or deltas with flooded vegetation (Ayoub et al., 2018; Jensen et al., 2021; Z. Zhang et al., 2017). All available ABoVE UAVSAR flight dates from non-contiguous days during summers 2017-2019 were used. Both early (June) and late (August-September) summer images were acquired by UAVSAR in 2017, and only late summer/early autumn dates were imaged in 2018 and 2019.

2.2.2 Water and land cover maps

Several ABoVE land cover data sets were referenced to help build a land cover training dataset for UAVSAR (see **Section 2.3.1**). High-resolution imagery and derivative water masks were obtained from the AirSWOT color-infrared camera (Kyzivat et al. 2018; Kyzivat et al. 2019; Kyzivat, et al. 2020), supplemented by high-resolution satellite imagery from Maxar (https://evwhs.digitalglobe.com/myDigitalGlobe/). Two satellite-based land cover maps available for the ABoVE domain were also referenced (Bourgeau-Chavez et al., 2017, 2019; Wang et al., 2019; Wang et al., 2019). Although these maps use a different classification scheme than our derived UAVSAR classification, they are particularly useful for partitioning between trees, shrubs, and graminoid vegetation.

2.3 Methods

2.3.1 Land cover classification training dataset

To estimate littoral zone extent, we aimed to develop a land cover classifier focused on emergent lake vegetation, which only grows in littoral zones. A training dataset was created using inundation status from field measurements in 2015 and 2017-2019 and vegetation categories from ABoVE land cover maps (Bourgeau-Chavez et al., 2017, 2019; Wang et al., 2019; Wang et al., 2019). As part of the field measurements, lake and wetland shorelines and vegetation zones were mapped by field teams carrying handheld GPS receivers, as described in Kyzivat et al. (2019). In YF, airborne GPS tracks from a low-hovering helicopter were used, as no suitable ground GPS tracks were available. Contextual photos were also taken by camera, both from the ground and from aircraft windows, and by uninhabited airborne vehicles (UAVs). UAV photos were processed into orthomosaics using DroneDeploy web software. All of these measurements were digitized into polygon shapefiles in ArcGIS 10.6 denoting 13 land cover classes falling into five broad categories of open water, dry land and three types of emergent macrophytes (**Table 1)**. The resulting vector data set (Kyzivat et al., 2021) was used to train and validate a supervised classification from the radar data.

Broad Grouping	**UAVSAR land cover class**
Open surface water	Open Water (OW), Rough Water (RW), Sedimentary Bar (SB), Wet Herbaceous (WH)
Wet Graminoid	Wet Graminoid (WG)
Wet Shrub	Wet Shrub (WS)
Wet Forest	Wet Forest (WF)
Dry land	Dry Graminoid (DG), Dry Shrub (DS), Dry Forest (DF), Bank Scarp Double-Bounce (BS), Dry Woodland (DW), Bare Ground (BG)

Table 1. Classification Schema: RW refers to wind roughening at the time of acquisition. WG refers to cattails (*Typha latifolia*), bulrushes (*Scirpus* spp.), and sedges (*Carex* spp.), as well as aquatic horsetails (*Equisetum fluviatile*). WS typically refers to willows (*Salix* spp.). DW refers

to a mix of trees and shrubs as defined by Wang (2019). WH refers to water lilies (*Nuphar variegatum*), and both WH and SB were not separable from the other open water classes. Further details are in the accompanying data publication (Kyzivat et al., 2021).

2.3.2 Synthetic aperture radar data pre-processing

UAVSAR GRD data for the PAD, YF and CSB flight lines were transformed to the C3 complex covariance matrix using PolSAR Pro 6.0 software. Images were corrected for incidence angle-dependent backscatter using a fitted exponential function multiplied by the cosine of incidence angle as per Ulander (1996) and Zhang et al. (2017). Due to its more rugged topography, CSD was corrected for both incidence angle and terrain slope as per the look-up table method of Simard et al. (2016). For all flight lines, a Freeman-Durden polarimetric decomposition was performed. The decomposition comprises a physical scattering model and is commonly used to identify scattering mechanism contributions to each pixel (single bounce, modeled as Bragg scattering; double bounce, modeled as from a pair of orthogonal surfaces; and volume scattering, modeled as from a cloud of randomly-oriented dipoles) (Freeman & Durden, 1998). Although it is known to overestimate the double bounce component (Chen et al., 2014), it is sufficient as an input feature to an empirical, machine-learning based classification.

2.3.3 Land cover classification

Each of the three scattering mechanism output bands was used for feature extraction via three moving-window filters designed to introduce spatial contextual information for the classifier. The chosen filters were standard deviations, offsets oriented along the radar look direction, and an edge-preserving guided filter to reduce speckle (**Table S.2**). Additional input bands of incidence angle and elevation-derived indexes were tested, but ultimately omitted, due to their high spatial autocorrelation, which led to model over-fitting. The training class BS was developed specifically to identify bright double bounce scattering between water surfaces and steep bank scarps, which would otherwise have appeared as inundated vegetation. SB and WH (defined as protruding <20 cm from the water surface, as determined from field measurements) were found to be inseparable from OW, so they were treated as open surface water in the analysis. The radar dataset was further prepared for classifier training by randomly under-sampling the majority training classes and cropping out pixels taken at low incidence angles. Incidence angle limits as well as filter parameters (**Table S.2**) were chosen by trial and error. Finally, pixel values within training polygons in all input bands from the appropriate date were extracted, and the results split using stratified sampling into training (85%) and validation (15%) datasets with 15 bands each. A description of this workflow, parameter settings, and other technical details is provided in the accompanying data publication (Kyzivat et al. 2021).

Finally, a random forests classifier was trained using the TreeBagger function in Matlab R2017b and evaluated using the validation dataset via the confusion matrix and Cohen’s kappa coefficient. One model was used for the areas with incidence angle correction and another for the CSD area with the look-up table correction. The models were then applied over the extent of their corresponding study areas for all available dates. The original 13 classes were aggregated into the five generalized classes for analysis (**Table 1**).

2.3.4 Quality control and conversion to vegetated littoral coverage

The derived five-class land cover maps were used to identify lake littoral zones and open water areas and quantify their total landscape coverage. First, maps were clipped to the intersection of all flight lines per study area excluding any roads or urban areas, if present. Raster mosaics were created for the PAD and YF, since they were acquired in multiple flight lines on most dates (**Table S.1**). Next, candidate lakes were identified as connected pixel groups of at least five pixels with at least one open water pixel and any number of inundated vegetation pixels (or none at all). This criterion permitted inclusion of open water wetlands, since there is no reliable way to differentiate them from lakes and ponds. Rivers were removed by applying a manually-created river mask, modified from Kyzivat et al. (2019). Littoral zones were operationally defined as emergent macrophyte classes 8-connected to lakes, with the remaining emergent macrophyte pixels considered wetlands. Although dependent on pixel size, this definition permitted a consistent definition, valid across all study areas. At this stage, the total landscape coverage of lake littoral zones (wet graminoid, shrub, and forest classes) and open water were calculated so they could be compared between dates.

Then, to calculate coverage on a per-lake basis, lakes smaller than 250 m^2 (0.00025 km^2 or 7-8 px) were discarded, since they were too small to consistently resolve and likely included false detections. Although hardly affecting total lake area, spurious lakes caused by false detections would be disproportionately small and thus impact the distribution of lake macrophyte coverages. Partially observed lakes intersecting the flight line boundary were discarded as well, since fractional macrophyte coverage could not be reliably measured. A third category of lakes were discarded if they did not overlap with any water pixels in the 2017 AirSWOT color-infrared camera open water masks, which had a slightly narrower ground footprint in all study areas. By comparing our UAVSAR retrievals to an independent, optical data set, this step removed many falsely-identified lakes caused by classification error. Finally, we calculated the areas of the remaining lakes and the fractional area of their vegetated littoral zones (A_{VL}), i.e., emergent macrophyte coverages, defined as the proportion of pixels in a lake classified as any of the three inundated vegetation classes. For visualization and analysis, these data were divided into 24 logarithmically-spaced lake area bins across the four study areas, and the mean, lake area-weighted mean, and median A_{VL} computed for each study area. For each study area, confidence intervals were calculated for each of the 24 bins and for the area-weighted means using the 95th percentile of 10,000 bootstrapped simulated datasets.

2.3.5 Methane flux chamber measurements

Methane flux chamber measurements were collected at 15 lakes in the PAD during July and August 2019 (Kyzivat et al. 2021, **Figure S.6**). In all 15 lakes, fluxes were taken from an open water region near the lake center via inflatable raft, anchored canoe, or motorboat. In five lakes, one to three additional flux measurements were made amidst macrophytes short enough to fit into the flux chamber without excessive disturbance. The chamber comprised an inverted 25.4 cm tall bucket with a 34.2 cm diameter opening wrapped with a buoyant skirt made of foam tubing. An infrared greenhouse gas analyzer (EGM-4, PP Systems) was used to measure chamber air carbon dioxide (CO_2) concentration and circulate chamber air via an inlet on the side of the chamber and an outlet in the center of its ceiling. A metal handle was used to steady the bucket for a 15-minute measurement period. At 0, 5, 10, and 15 minutes, gas samples were drawn from the chamber's headspace through the gas analyzer inlet tubing and injected into evacuated exetainers using a 30 mL polypropylene syringe fitted with a 3-way stopcock for subsequent analyses of methane concentration.

The samples were analyzed on a Shimadzu GC-2014 gas chromatograph for methane partial pressure within two months of collection. Gas flux across the water-air interface was calculated from the rate of change in the chamber methane concentration over the deployment time and chamber area ($mol \cdot min^{-1} \cdot m^{-2}$). The rates of change of methane concentrations in the chamber were generally linear with r^2 values greater than 0.90. Given this linear response, ebullition was deemed negligible during the measurement periods. Thus, the closed, static chamber measurements included both diffusive fluxes from the water surface as well as any plant-based fluxes. When multiple fluxes were taken at one location, measurements from each water zone were averaged by lake. Finally, for sites where paired open water vs. littoral zone measurements were collected, we calculated the littoral:pelagic flux ratio (hereafter: flux ratio) as the ratio between the average emergent macrophyte and open water measurements for each lake.

During sampling, care was taken not to disturb the sediment, and if any bubbles were observed before or during the period, the measurement was aborted. Even so, three measurements were extremely high, implying sediment disturbance. To avoid potential bias, these measurements, which were greater than 2.2 standard deviations from the median, were discarded (the next-highest value was 0.17 standard deviations from the median). These three measurements all came from vegetated sites, so this data omission lessened the impact of emergent vegetation in our subsequent analyses.

2.3.6 Published flux chamber measurements

In addition to our own field measurements, we compiled a synthesis dataset of 44 paired lake center (pelagic zone) and littoral zone flux measurements, with the aim of determining the flux ratio for each lake. Each pair corresponded to one of 38 distinct lakes or lake regions during a single or multi-year-averaged sampling season, published in 14 papers (Kankaala et al. 2005; 2013; Smith and Lewis 1992; Larmola et al. 2004; Huttunen et al. 2003; Juutinen et al. 2003; Villa et al. 2021; Burger et al. 2016; DelSontro et al. 2016; Bergström et al. 2007; Striegl and Michmerhuizen 1998; Ribaudo et al. 2012; Casper et al. 2000; Dove et al. 1999) (**Supplementary Table 1**). Lakes included boreal, tropical and temperate regions and are located in Finland, Quebec, Colorado, Ohio, Minnesota, Italy, the UK, and the Amazon and Orinoco river basins. For each paper, the average—whether seasonal or annual—littoral and pelagic measurements were recorded and converted, if necessary, to units of mg CH_4/m^2/day. Three papers (Burger et al., 2016; Casper et al., 2000; Dove et al., 1999) separately measured each of the three methane emission pathways, and most of the others focused on diffusion and/or plant-based fluxes. An additional three (Huttunen et al., 2003; Juutinen et al., 2003; Villa et al., 2021) measured diffusion and ebullition in both lake zones, but did not place the flux chamber over plants, thus not accounting for that pathway. One study (Bergström et al., 2007) did not provide open water values, so values were estimated based on lake area via the relationship of Holgerson and Raymond (2016). The compiled dataset therefore includes measurements of three methane flux pathways collected from both littoral vegetation and shallow open water.

Many papers stated the area covered by emergent macrophytes, but if not, Google Earth Pro and QGIS 3.10.11 were used to digitize, map project, and measure the approximate coverage area, with attention paid to the papers' description of the vegetation for context. Coverage areas were assigned an uncertainty value (typically 2–5%) based on interpretation of the methods used or confidence in our digitizing result. Although challenging to compare across methodologies, geographic regions, and plant types, this dataset served as a best estimate of flux ratios from a diverse global sample of lakes.

2.3.7 Sensitivity analysis

Likely ranges in whole-lake methane emissions were calculated using the following equation and the compiled flux dataset:

$$f_{total} = A_{VL} * f_{VL} + (1 - A_{VL}) * f_{OW} \qquad [1]$$

where A_{VL} is the fractional vegetated littoral area per lake, f_{VL} is the corresponding flux per unit area, and f_{OW} is the flux from open water. The littoral zone impact on whole-lake flux (relative to an estimate assigning open water flux values to the entire lake) was calculated as:

$$I = \frac{f_{total} - f_{OW}}{f_{OW}} \qquad [2]$$

where *I* represents the percent increase from including littoral zones.

Equation **[2]** was applied using the median values of f_{VL} and f_{OW} and the lake area-weighted mean A_{VL}. Median values were used due to the skewed distributions of f_{VL}, f_{OW} and the flux ratios. The equation was also applied to the bootstrapped confidence intervals of A_{VL} in order to estimate uncertainty.

3 Results

3.1 Inundation patterns at the landscape scale

3.1.1 Regional and seasonal inundation characteristics

Significant open water, littoral zone, and wetland fractional areas are found in all study areas, vary seasonally as well as regionally, and are particularly extensive in the PAD and YF. The total area of the landscape covered by vegetated littoral zones varies from 0.5 – 0.6 % (CSD), 2.2 – 3.4 % (CSB), 7.6 – 15.5 % (PAD), and 1.7 – 2.8 % (YF) over the 2017-2019 observational period (**Figure 2, Table 2**). In comparison, non-littoral, or wetland, emergent vegetation (A_{WV}) covers ≤ 2.7% of the area in all sites (mean of 1.4%, **Table 2**). Most of the emergent littoral vegetation area is classified as either wet graminoid (WG, weighted mean of 69%) or shrub vegetation (WS, 29%), with wet forest comprising <1% of this area for all areas except YF, for which it covers a mean of 5.9%. Virtually all detected vegetated littoral zones are adjacent to shorelines, with < 0.2% of their area occurring completely within a lake with no connectivity to non-island land. These patterns show that the dominant littoral vegetation type in the study areas is graminoids, which almost always occur at the interface between land and water.

In all applicable study areas, total inundation (open water plus vegetated littoral zones) is greater or equal in the early summer (June) than in late summer (August/September), likely due to the effects of recent snowmelt and soil thawing. In the PAD, this change is caused by decreased littoral vegetation, with inundated wetland vegetation remaining constant, implying that seasonal inundation changes occurred in flood-tolerant eulittoral vegetation (**Figure 2, Table 2**). Thus, regional variations in emergent vegetation, as well as open water, are greater than seasonal/interannual variations within study areas.

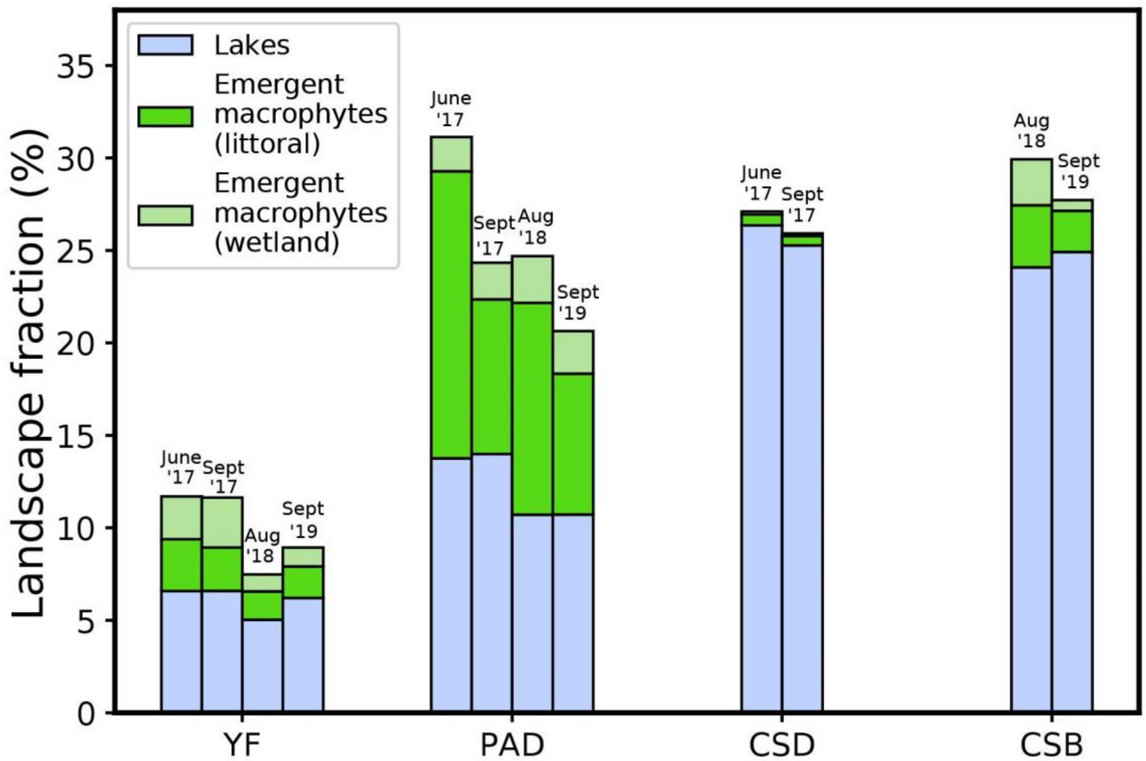

Figure 2. Significant littoral zone fractional areas are found in all study areas, vary seasonally as well as regionally, and are particularly extensive in the lowland PAD and YF. This chart shows landscape fractional areas of open water and emergent macrophyte classes for the Yukon Flats (YF), Peace-Athabasca Delta (PAD), Canadian Shield – Daring Lake (CSD), and Canadian Shield – Baker Creek (CSB), derived from airborne UAVSAR. Littoral zones are defined as emergent macrophytes adjacent to open water, with remaining areas assigned to wetlands. Month

and year of UAVSAR flight acquisitions appear in text above each column.

				Lake fraction (%)						Landscape area (km^2, %)					
	Study area	Area (km2)	Lake count	A_{VL}	A_{WF}	A_{WS}	A_{WG}	A_{VL} (median)	A_{VL} (unweighted)	Water	A_{VL}	A_{WF}	A_{WS}	A_{WG}	Vegetated wetland
CSD June 2017	CSD	3037	1918	1.1 [0.9, 1.4]	0.0 [0.0, 0.0]	0.0 [0.0, 0.1]	1.1 [0.9, 1.3]	0.0%	2.0%	800 (26.4%)	18 (0.6%)	0 (0.0%)	1 (0.0%)	17 (0.6%)	3 (0.1%)
CSD Sept 2017	CSD	3037	1975	0.9 [0.6, 1.1]	0.0 [0.0, 0.0]	0.0 [0.0, 0.0]	0.8 [0.6, 1.1]	0.0%	3.8%	767 (25.3%)	16 (0.5%)	0 (0.0%)	0 (0.0%)	15 (0.5%)	2 (0.1%)
CSD		3037	1947	1.0 [0.8, 1.2]	0.0 [0.0, 0.0]	0.0 [0.0, 0.1]	1.0 [0.7, 1.2]	0.0%	2.9%	784 (25.9%)	17 (0.5%)	0 (0.0%)	1 (0.0%)	16 (0.5%)	3 (0.1%)
CSB Aug 2018	CSB	1155	376	8.6 [5.8, 14.1]	0.0 [0.0, 0.1]	2.3 [1.7, 3.6]	6.2 [4.1, 10.5]	20.4%	26.6%	278 (24.1%)	39 (3.4%)	0 (0.0%)	11 (1.0%)	28 (2.4%)	29 (2.5%)
CSB Sept 2019	CSB	1160	378	5.5 [3.6, 9.0]	0.0 [0.0, 0.1]	0.7 [0.5, 1.1]	4.7 [3.1, 7.9]	11.3%	17.5%	289 (24.9%)	26 (2.2%)	0 (0.0%)	4 (0.3%)	22 (1.9%)	7 (0.6%)
CSB		1158	377	7.0 [4.7, 11.5]	0.0 [0.0, 0.1]	1.5 [1.1, 2.3]	5.5 [3.6, 9.2]	15.9%	22.1%	284 (24.5%)	32 (2.8%)	0 (0.0%)	7 (0.6%)	25 (2.1%)	18 (1.5%)
PAD June 2017	PAD	1339	347	65.5 [56.5, 75.3]	0.7 [0.2, 1.3]	35.3 [28.2, 42.6]	29.5 [21.4, 38.8]	63.5%	58.3%	184 (13.8%)	[illegible]08 (15.5%)	2 (0.1%)	73 (5.4%)	33 (10.0%)	25 (1.8%)
PAD Sept 2017	PAD	1338	729	52.1 [42.8, 61.6]	0.1 [0.0, 0.3]	13.8 [9.0, 19.5]	38.2 [31.4, 45.3]	60.5%	56.2%	187 (14.0%)	112 (8.4%)	0 (0.0%)	18 (1.3%)	94 (7.0%)	26 (1.9%)
PAD Aug 2018	PAD	1338	366	61.4 [51.8, 70.8]	1.1 [0.3, 1.9]	39.3 [31.1, 47.6]	21.1 [15.8, 27.7]	68.4%	62.0%	143 (10.7%)	153 (11.4%)	1 (0.1%)	64 (4.8%)	88 (6.6%)	34 (2.5%)
PAD Sept 2019	PAD	1336	437	56.6 [49.2, 65.2]	0.3 [0.0, 0.6]	33.3 [26.9, 40.2]	22.9 [16.8, 31.1]	57.1%	57.7%	143 (10.7%)	102 (7.6%)	0 (0.0%)	42 (3.1%)	60 (4.5%)	31 (2.3%)
PAD		1338	470	58.9 [50.1, 68.2]	0.6 [0.1, 1.0]	30.4 [23.8, 37.5]	27.9 [21.3, 35.7]	62.4%	58.6%	164 (12.3%)	144 (10.7%)	1 (0.1%)	49 (3.7%)	94 (7.0%)	29 (2.1%)
YF June 2017	YF	2739	2687	24.9 [22.8, 27.2]	1.2 [0.2, 2.5]	4.0 [3.4, 4.8]	19.7 [18.0, 21.6]	31.8%	36.8%	180 (6.6%)	77 (2.8%)	4 (0.1%)	14 (0.5%)	58 (2.1%)	63 (2.3%)
YF Sept 2017	YF	2739	2857	22.6 [20.7, 24.7]	1.3 [0.3, 2.6]	5.5 [4.3, 6.8]	15.8 [14.6, 17.3]	27.0%	33.5%	180 (6.6%)	64 (2.3%)	4 (0.1%)	15 (0.6%)	45 (1.6%)	74 (2.7%)
YF Aug 2018	YF	2739	1784	22.4 [19.7, 25.3]	1.8 [0.3, 3.8]	4.6 [3.6, 6.0]	16.0 [14.3, 17.9]	17.0%	28.2%	138 (5.0%)	42 (1.5%)	3 (0.1%)	10 (0.4%)	30 (1.1%)	25 (0.9%)
YF Sept 2019	YF	2739	1533	18.5 [16.1, 21.2]	1.9 [0.4, 4.0]	2.3 [1.8, 3.0]	14.3 [12.7, 16.1]	15.6%	25.5%	170 (6.2%)	47 (1.7%)	3 (0.1%)	9 (0.3%)	35 (1.3%)	28 (1.0%)
YF		2739	2215	22.1 [19.8, 24.6]	1.5 [0.3, 3.2]	4.1 [3.3, 5.2]	16.5 [14.9, 18.2]	22.8%	31.0%	167 (6.1%)	57 (2.1%)	3 (0.1%)	12 (0.4%)	42 (1.5%)	47 (1.7%)
Mean				22.3 [18.9, 26.4]	0.5 [0.1, 1.1]	9.0 [7.1, 11.3]	12.7 [10.1, 16.1]	25.3%	28.6%	350 (17.2%)	63 (4.0%)	1 (0.1%)	17 (1.2%)	44 (2.8%)	24 (1.4%)
Weighted mean				16.2 [13.9, 19.1]	0.5 [0.1, 1.1]	5.8 [4.5, 7.2]	10.0 [8.2, 12.2]	17.9%	21.8%	409 (16.9%)	53 (3.0%)	1 (0.1%)	13 (0.8%)	38 (2.1%)	24 (1.2%)
Mean (late summer)				21.4 [18.0, 25.6]	0.5 [0.1, 1.1]	8.6 [6.7, 10.9]	12.3 [9.8, 15.5]	24.4%	28.4%	343 (16.9%)	55 (3.6%)	1 (0.0%)	15 (1.0%)	39 (2.5%)	23 (1.3%)
Weighted mean (lt. s.)				15.0 [12.7, 17.8]	0.5 [0.1, 1.1]	5.3 [4.1, 6.7]	9.2 [7.5, 11.3]	16.4%	21.1%	401 (16.6%)	47 (2.7%)	1 (0.0%)	12 (0.7%)	34 (1.9%)	22 (1.1%)

Table 2. Within-lake vegetated littoral zone coverages (A_{VL}) by vegetation type (A_{WF} = area of wet forest, A_{WS} = area of wet shrub, A_{WG} = area of wet graminoid, A_{WV} = area of wetland vegetation, as opposed to littoral vegetation) and by study area, along with landscape coverage in square kilometers and as percent coverages. Numbers in brackets give the bootstrapped 95% confidence intervals. Weighted mean columns are weighted by individual lake area, and summary weighted mean rows are weighted by the total lake area of each study area for all dates and late summer only (August and September, abbreviated as lt. s. when necessary).

3.1.2 Validation of UAVSAR classifier

The land cover classifier successfully retrieves the three broad classes of emergent vegetation. Based on visual inspection of the land cover maps, the most significant misclassification is evidenced by false detections of water in areas actually covered by dry graminoid vegetation (**Figure 3e**, top middle) and false detections of inundated vegetation in areas of forest. The most frequent misclassification occurs between Wet Shrub and Rough Water, although errors of omission and commission are roughly equal, implying a near-zero net effect on the landscape totals (**Figure S.1**). Any misclassification among the dry land classes does not affect our lake analysis, and misclassification between the flooded and dry classes is rare, as expected, given the sensitivity of SAR to water presence (**Figure S.1**). Prior to the quality control measures (**Section 2.3.4**), Cohen's kappa coefficients are 0.862 for the model used on the simpler CSD landscape and 0.824 for the model used for the remaining sites, implying good agreement with the validation data. Since the analysis only uses flooded classes connected to open water that could be validated by optical imagery, errors of commission (**Figure S.1**) represent an upper bound.

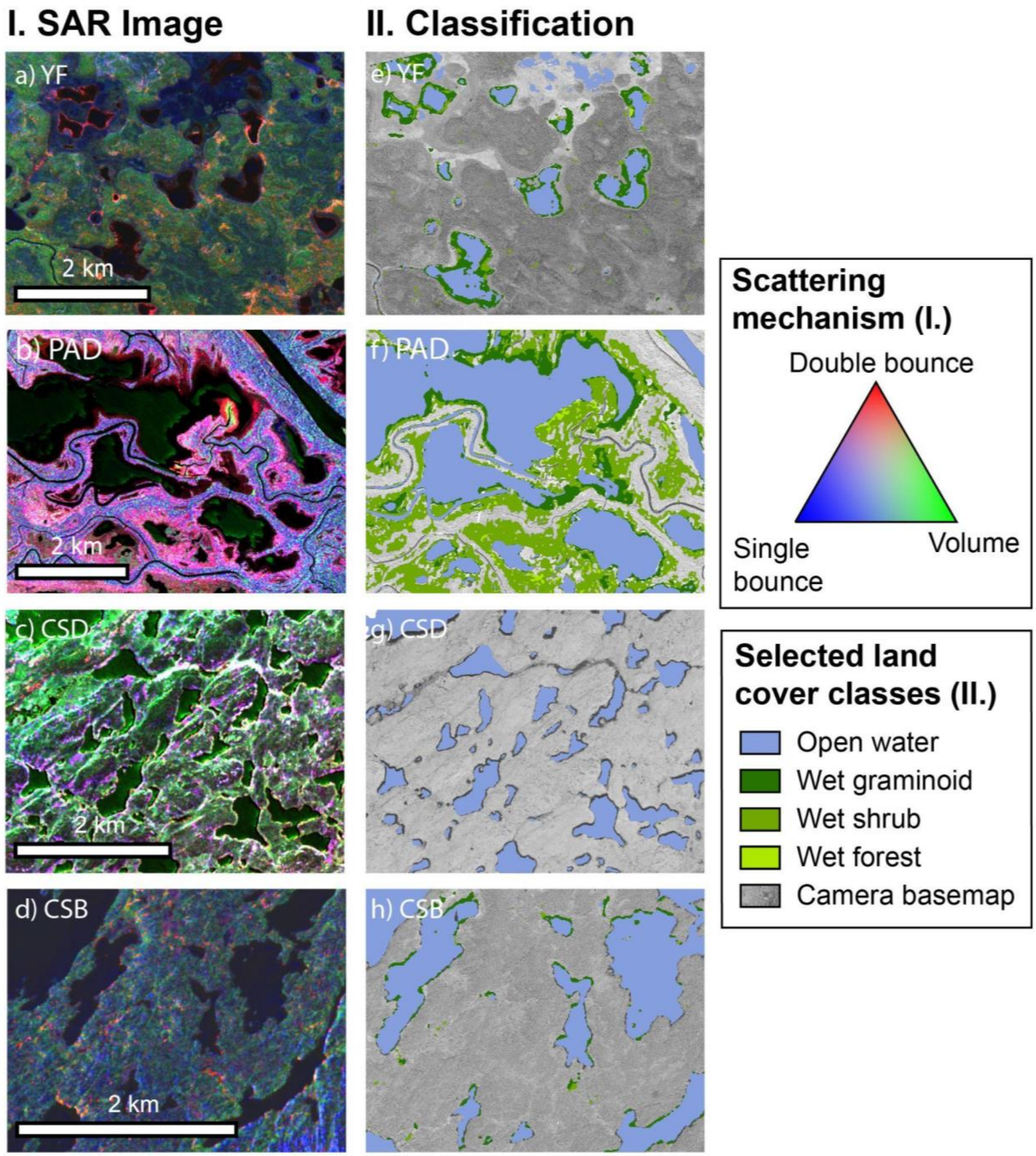

Figure 3. Example L-band SAR images of subsets within the four study areas (**Colum I. a-d**, YF 6/2017, PAD 9/2019, CSD 9/2017, CSB 8/2018, respectively) and corresponding classification (**Column II. e-h**). SAR images are colorized by Freeman-Durden scattering mechanism (double bounce in red, primarily indicating emergent macrophytes; volume scattering in green, primarily indicating leafy vegetation; and single bounce scattering in blue, primarily indicating bare ground, bedrock, and some types of trees) and are stretched identically, with visual adjustments for brightness and color saturation. In column **II**., only inundated classes are shown and are

superimposed over a grayscale version of the color-infrared camera base map from Kyzivat et al. (2018), in which forests appear darker than grasslands or bedrock.

3.2 Vegetated littoral zone extent

3.2.1 Regional and morphological trends

Although useful for integrating all flux components, landscape-scale descriptors obscure the nuance of individual lake characteristics. Consequently, we also present results normalized by each lake's area and aggregated via weighted averaging (**Table 2, Figure 4**). With this normalization, it is more apparent that vegetated littoral zones (A_{VL}) are quite prevalent in lakes, averaging 16.2 [13.9 – 19.1]% across the four study areas, weighted by lake area. Again, coverage is especially extensive in the lowland PAD and YF (**Figure 2**), averaging 59 [50 - 68]% and 22 [20 – 25]%, respectively. A_{VL} in the more topographically constrained, colder, sparsely vegetated CSB and CSD areas averages 7.0 [4.7 – 11.5]% and 1.0 [0.8 – 1.2]%, respectively. The lowland sites, therefore, have the most A_{VL}, both as a percentage of total lake area as well as landscape area.

While vegetated littoral zones are observed in every size bin in every area, we find only a weak relationship between A_{VL} and lake area that holds for all study areas. The area bins comprising small to medium-sized lakes between 0.002 to 0.02 km^2 always contain the primary histogram peak, with the exception of the PAD, for which these bins contain the secondary peak (**Figure 4b**). In all regions except the PAD, the smallest observable lakes ($\geq$ 250 m^2) have similar coverage to the largest (> 10 km^2), resulting in unimodal area-binned histograms, even within the confidence intervals (**Figure 4**). The drop in A_{VL} for small lakes is likely caused by mixed pixels in narrow littoral zones being detected as water. Even so, Pearson correlation is weak between log-transformed A_{VL} and lake area ($r^2 = 0.124$, $p < 0.001$, **Figure 5**), implying that the inverse relationship between the two variables is not consistent across sites. On an individual basis, the two Canadian Shield study areas have significant regression relationships ($p < 0.001$, **Figure 5**), with $r^2 = 0.25$ (CSB) and 0.48 (CSD), likely explained by their simpler, bedrock-dominated landscapes.

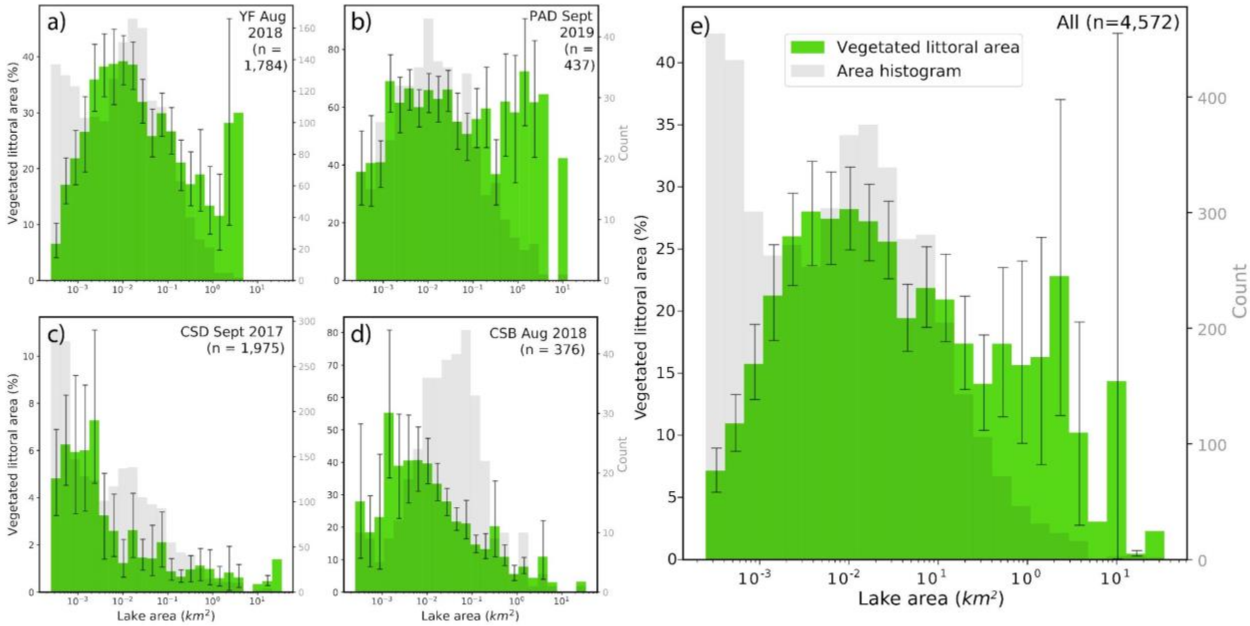

Figure 4. Vegetated littoral zones (A_{VL}) are most prevalent in small to medium-sized lakes. Here, mean A_{VL}, in green, is calculated for logarithmic lake area bins for each region (a) and for all regions combined (b). Error bars give the 95% confidence interval for A_{VL} for all bins with > 2 observations. The lake count in each bin is plotted in grey and shows that most observed lakes are much smaller than 1 km^2. Accordingly, bins with fewer lakes generally have greater uncertainty in A_{VL}, and the rightmost bins, which contain < 10 lakes, have considerable uncertainty. For a version of this figure showing bin sums, rather than means, see **Figure S.2**.

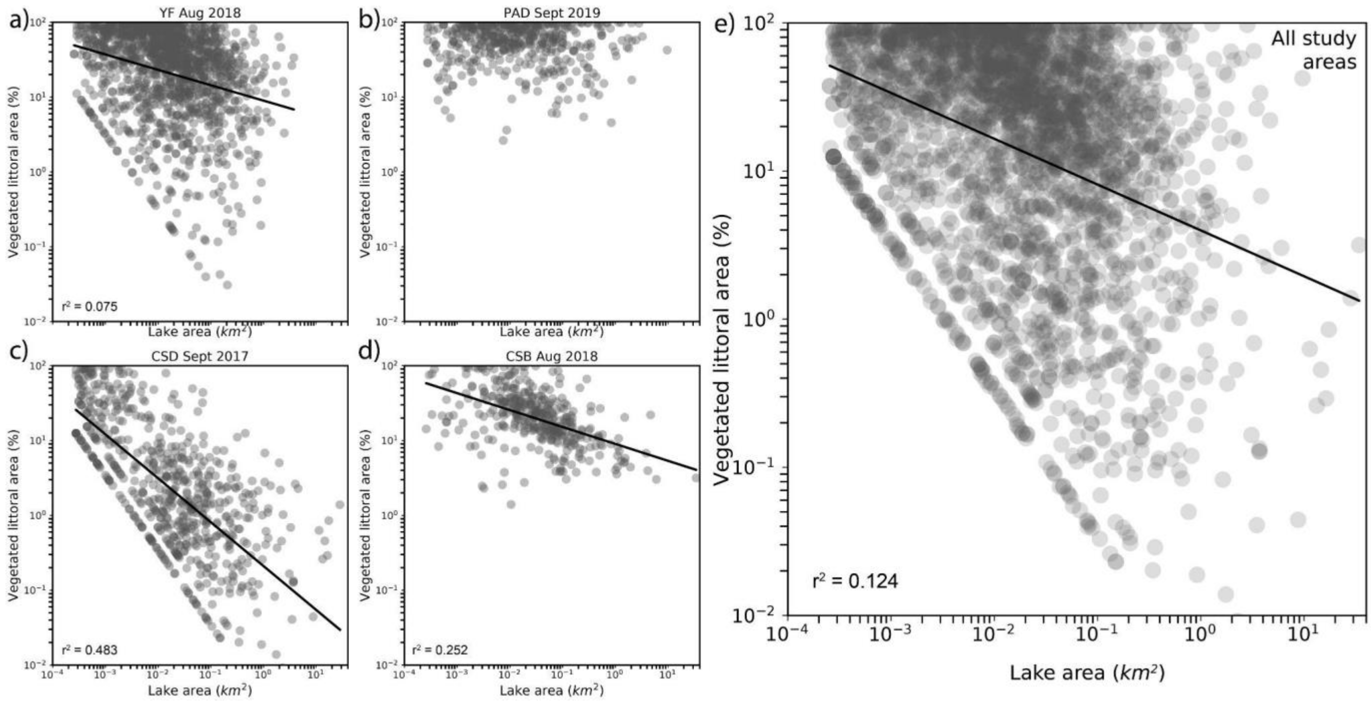

Figure 5. Scatter plot of lake area and emergent macrophyte coverage (A_{VL}) for all 4,572 lakes by study area (**a-d**) and aggregated (**e**). There is only a weak relationship between the two log-transformed variables. The diagonal bottom-left boundary in most plots is caused by area quantization by pixilation; since A_{VL} is a fraction, the minimum possible A_{VL} corresponding to a one-pixel littoral zone decreases as the denominator increases. Lakes with $A_{VL} = 0$ are not shown nor included in the regression and regression lines are only included for $p < 0.001$.

3.2.2 Seasonal trends

Despite fluctuating water levels, the distribution of A_{VL} remains largely similar across seasons and years (**Figure S.3**). In all study areas, there is a histogram peak at lakes with little or no vegetated littoral zone (**Figure S.3 a-d**, leftmost bin), as many areas lack the necessary conditions to support emergent macrophytes. The histogram drops sharply with increasing A_{VL} coverage: extremely quickly in the sparsely-vegetated CSD, somewhat quickly in the more southern CSB, and gradually in YF. The negative-skewed PAD distribution (tail on left) is an anomaly with high-coverage lakes common. Accordingly, the area-weighted mean (58.9 %) is barely greater than the arithmetic mean coverage (58.6 %) in the PAD, unlike the rest of the study areas and the aggregated total, for which these values can differ by a factor of two (**Table 2**). There are also more lakes overall detected in the PAD during early summer (**Figure S.3**), likely because temporarily submerged macrophytes would be detected as open water and thus constitute lakes in our analysis. These effects are likely due to prevalence of shallow open water wetlands, which are ubiquitous in the delta and are included in our lake dataset as long as some area of open water (> one pixel, or ~30 m^2) is detected. The temporal invariance of the A_{VL} histograms provides further validation of the consistency of the classifier, and it shows how changes in A_{VL} are not relegated to the same small subset of lakes.

3.3 Methane fluxes from vegetated littoral zones vs. open water

Field measurements confirm that methane fluxes from emergent macrophytes are consistently higher than open water, even within the same lake (**Figure 6**). Although macrophyte fluxes were only collected at five of the visited PAD lakes, four had higher mean macrophyte values than open water, leading to a mean macrophyte: open water flux ratio of 2.7. The fluxes obtained by literature synthesis have an even more extreme median ratio of 8.0 (**Figure 7**, top histogram). Of the 44 paired measurements, all but seven have flux ratios > 1. The PAD and literature measurements combined have a median flux ratio of 6.2, or 5.9 if only Arctic-boreal lakes are included. We use the latter, smaller value for the subsequent sensitivity calculation. Despite a limited and spatiotemporally uneven global sampling, lakes in our study areas and worldwide significantly trend towards higher emissions from vegetated littoral zones (paired t-test, $t = 6.5$, $p < 0.001$.

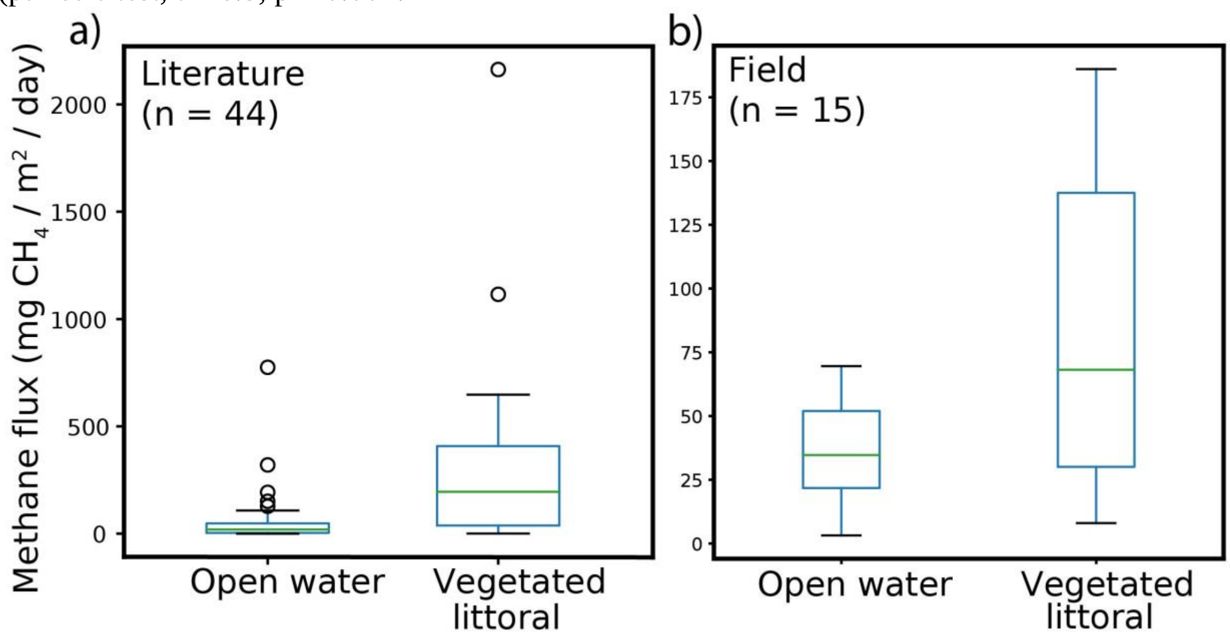

Figure 6. Vegetated littoral zones produce greater methane fluxes than open water zones based on the literature (**a**) and from field measurements in the Peace-Athabasca Delta in July and August 2019 (**b**). Green lines show the median, hinges are drawn at the lower and upper quartiles, and flyer bars give the extent of data not considered outliers, which are plotted as points. Note the different scales demonstrating much greater flux values (mg of CH_4 /day) from the literature (**a**) than in the PAD (**b**).

3.4 Sensitivity of whole-lake methane emissions to inclusion of littoral zone areas

By applying the median Arctic-boreal macrophyte:open water ratio of 5.9 (**Figure 7**) to our remotely sensed UAVSAR littoral maps (**Figure 3**), we estimate the relative importance of accounting for vegetated littoral zones in whole-lake methane flux estimates. Assuming a lake area weighted average A_{VL} of 16.9 [13.9 - 19.1]% increases the overall methane emissions from the four study areas by 79 [68 – 94]% (**Figure 7**). Spatiotemporally, this ratio I, varies from 4% to 321%, with the lower bound coming from CSD in September 2017 (where only ~0.9% of lake areas have vegetated littoral zones) and the upper bound from the PAD in June 2017 (~66% coverage, **Table 2**). Although these are the most extreme values observed, these scenarios show that accounting for even small littoral zone areas significantly raises whole-lake emissions estimates.

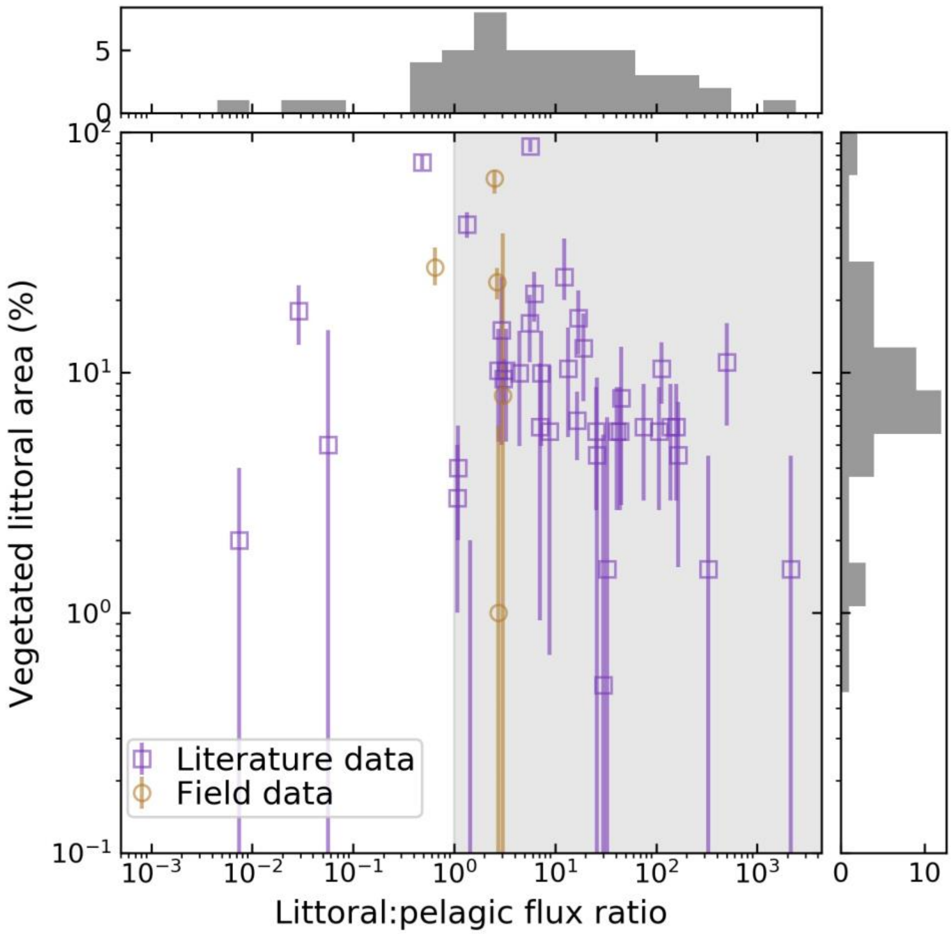

Figure 7. Plotting study lakes in a flux ratio-littoral vegetation fraction feature space shows that most would have higher calculated fluxes (shaded area) if their littoral zones are accounted for separately from open water, with median increase of 79%. The distributions of both variables are shown as histograms along the relevant axes. Vertical error bars show the temporal range in coverage for the field data (orange circles) and the estimated mapping uncertainty for the literature data (purple squares) and can extend to zero (beyond axis limits). For scale, the uppermost data point in the figure (Lake Mekrijärvi, Finland) corresponds to a 56-fold increase in emissions compared to the no littoral zone case. Note the logarithmically-scaled x and y axes. For a version of this figure with contour lines showing how much higher this calculated flux would be, see **Figure S.4**.

4 Discussion and Conclusion

4.1 Littoral zone coverage in lakes

Littoral zones are often theorized to cover greater portions of small lakes than large (Bergström et al., 2007; Wetzel, 1990, 2001). It is logical that smaller lakes with larger perimeter:area ratios would be dominated by near-shore areas, which are overwhelmingly shallow. However, while our results generally show greater fractional vegetated littoral area (A_{VL}) in small and medium-sized lakes (**Figure 4**), there is weak correlation at best (Pearson r^2 = 0.124, $p < 0.001$; **Figure 5**). This discrepancy can likely be explained by emergent macrophytes comprising only a portion of the littoral zone, as well as mixed pixels obscuring narrow littoral margins in small lakes. Bergström et al. (2007) similarly observed that medium-sized lakes (0.1 to 1 km^2) had the greatest A_{VL} of ~11% on average for 50 Fennoscandian Shield lakes in Finland, which, plotted as an area-binned histogram, also resembles an inverted V-shaped curve. Mäkelä et al (2004), using the same dataset, pointed out that large, lowland lakes had the largest total macrophyte coverage, also noting that area and pH only account for 15% variation in A_{VL}.

In comparison, the Canadian Shield areas we sampled contained the greatest A_{VL} in small-to-medium lakes (0.0001 - 0.002 km^2 in area), with values ranging from 7.3 [4.5 – 10.7] % (CSD) to 55 [35 – 81] % (CSB). We also observe a large contribution to total littoral zone area from the large lakes (**Figure S.2**), underscoring the need not to discount them due to their small fractional A_{VL}. The largest 100 lakes (area ≥ 0.9 km2) comprise 62.7% of total lake area and 39.2% of total vegetated littoral area across all four study areas, and this trend holds across all study areas (**Fig S.2**). The observed region-specific dependence on lake area further highlights the need for remote sensing to accurately estimate littoral zone coverage.

The ~16% mean A_{VL} coverage we observe is greater than the globally-inclusive estimate of 7% (Duarte et al.,1986) and Southern Finland estimate of 5.2% (Bergström et al., 2007). Since the number is an intermediate average derived from much lower values on the Canadian Shield (1.0%, and 7.0% for CSD and CSB, respectively, **Table 2**) and much higher values for the PAD (59%) and YF (22%), it is highly sensitive to the choice of study areas and their relative sizes. Although the relationship between coverage and lake area does not appear as simple as suggested by Duarte et al. (1986), their conclusion that lake area is not a strong predictor of emergent macrophyte coverage is still supported. Clearly, A_{VL} coverage varies greatly across different areas, again highlighting the need for regionally-varying remote sensing products for methane upscaling.

4.2 Importance of vegetated littoral zones for methane upscaling

4.2.1 Toward improved upscaling of lake methane emissions

This broad-domain study supports previous studies demonstrating the importance of accounting for vegetated and/or littoral areas in upscaling lake methane flux estimates (Bergström et al., 2007; Casas-Ruiz et al., 2021; DelSontro, del Giorgio, & Prairie, 2018; Juutinen et al., 2003; Kankaala et al., 2013; Natchimuthu et al., 2016; L. K. Smith & Lewis, 1992; Striegl & Michmerhuizen, 1998). However, in addition to the challenges of measuring wetland extent more generally (Melton et al., 2013), a knowledge gap remains about the distribution and area of lake littoral zones (Huttunen et al., 2003). The airborne UAVSAR approach presented here has limited spatial coverage and is unsuitable for broader-scale studies.

Satellite approaches, however, have good utility for pan-Arctic or global wetland mapping (Hess et al. 1990, Nelson et al. 2006, Ghirardi et al. 2019, Zhang et al. 2021) and are well suited for study of large lakes, which contribute most to total vegetated littoral area (**Fig S.2**). These lakes are otherwise considered low methane emitters on a per-area basis (Holgerson & Raymond, 2016) and have little risk of being double-counted in wetland datasets, so they would be a good starting point for future studies. The upcoming NISAR satellite mission is likely to provide high-resolution, freely available global coverage of L-band SAR, which may facilitate similar analysis over larger scales.

Unfortunately, our results do not reconcile the gap between modeled methane fluxes from bottom-up and top-down models (Thornton et al. 2016). In fact, they suggest bottom-up fluxes are greater than previously thought, which further widens the discrepancy. With more, high-quality input data besides lake area, upscaling estimates can be made more nuanced, and ultimately, more accurate. Development of global mapping capacity focused on vegetated lake littoral zones could aid landscape scale modeling of methane emission processes and fluxes to the atmosphere.

4.2.2 Limitations and future directions

Our 79% estimate for I (**Equation 2**), the percent increase due to including vegetated littoral zones in lake methane flux accounting, is a conservative estimate influenced by a variety of assumptions and is most likely too low. First, our use of emergent macrophytes as a proxy for littoral zones can cause underestimation, since high littoral emissions are not solely restricted to vegetated regions. The floating-leaved macrophytes not detectable from UAVSAR, such as water lilies, can cover roughly equal areas, although typically with lower methane emissions (Bergström et al., 2007; Juutinen et al., 2003; Laanbroek, 2009). Non-vegetated littoral zones are also excluded from our mapping and upscaling estimate, but can be high emitters, especially when within the reach of carbon-exuding roots and rhizomes (Bansal et al. 2020). Furthermore, three of the studies in the synthesis dataset did not measure the plant-based emission pathway. Bansal et al. (2020) observed lower sediment pore water concentrations near plants than in a plant-free control in a mesocosm experiment, implying that the presence of a plant pathway can detract from the others, which suggests the three studies may have under-estimated the flux ratio. To the opposite effect, our estimate includes emergent shrubs and trees, which lack the aerenchyma tissue that allows most wetland plants to transport methane from the sediments. Recent work has shown the potential for microbes living inside trees to produce methane (Covey & Megonigal, 2019), although this effect is likely less than soil microbe production. Even so, like emergent graminoids, the presence of inundated trees indicates shallow water and abundant organic matter inputs, which are both drivers of methane emissions. Future work should develop remote sensing techniques that can more accurately quantify the ratio of emergent vegetation area to total littoral zone area.

Secondly, the estimate has the potential to be too high, since the relatively narrow swath width of UAVSAR causes large (and likely less-vegetated) lakes to be under-represented in the calculation of weighted mean A_{VL}. Adding to this effect is the use of the same littoral:pelagic flux ratio for lakes of all sizes, when smaller lakes and ponds are known to be higher open-water methane emitters than large (Michmerhuizen, Striegl, & McDonald, 1996; Bastviken et al., 2004; Holgerson & Raymond, 2016; Engram et al. 2020), probably because littoral zones (vegetated and unvegetated) cover most of their areas. Indeed, Kankaala et al. (2013) showed that the flux ratio increases with lake size. It follows that our concept of a littoral:pelagic flux ratio is less useful for small lakes, and would likely be even larger for the largest lakes, which were under-represented in our literature synthesis. Future studies could better quantify how this ratio varies based on lake area. Nevertheless, since the contribution to total A_{VL} from the small lakes is so slight (**Fig S.2**), they don't have a large negative impact on our estimate.

Finally, our estimate may be too low because it assumes that the vegetated littoral area not accounted for in open water upscaling estimates should come from what were considered open water regions. In reality, most global lake area estimates (Lehner & Döll, 2004; Verpoorter et al., 2014; Meyer et al., 2020) have relied indirectly on optical remote sensing, which is likely to exclude A_{VL}, which may appear as dry vegetation. Thus, it might be more realistic for a global upscaling estimate to use larger total lake areas to account for the unobserved vegetated littoral zones. One would have to use care to ensure that wetlands are being adequately accounted for and not double-counted (Thornton et al., 2016) with vegetated littoral zones. Littoral zones often have fluctuating inundation, and there are valid reasons to count them as either lakes or wetlands, which complicates upscaling efforts, which should be consistent. In the absence of a global lake littoral zone accounting, future studies could look at relationships between remotely-sensed measurements such as lake morphology, topography, and littoral vegetation, as well as other known factors that influence methane production.

Comparison of our sensitivity study with previous Arctic-boreal and global lake studies suggests that our finding of a 79% increase in whole-lake methane flux is conservative. Using flux chamber measurements from two Swedish lakes, Natchimuthu et al. (2016) found that methane emissions from lake centers are 2.1 times smaller than whole-lake fluxes. Similarly, Kankaala et al. (2013) found that 74-82% of methane emissions in 12 Finnish lakes derived from littoral macrophyte stands comprising only 5% of their total area. These amounts correspond to a flux ratio of 54-86, leading to an impact, *I*, on whole-lake fluxes between 270 and 430% greater than a case where pelagic fluxes were assumed throughout. The global estimate of Bastviken et al. (2011) implies a flux ratio of 43.2 for lakes and reservoirs, signifying *I* of 219 to 640 % for 5% to 15% A_{VL}, respectively. The high flux ratio derived from the latter two cases is likely due to the area-weighted analyses including much larger, and thus lower-emitting per unit area, lakes than our airborne-based study. Furthermore, our mean Arctic-boreal zone flux ratio of 5.9 is much smaller than the Finnish and global estimates, so more paired flux measurements are needed to better constrain these estimates. Thus, our estimate is conservative and the lowest of these three estimates, although all have different spatial and lake size domains.

4.3 Conclusion

Vegetated littoral zones are ubiquitous in Northern lakes but limited data prohibit their inclusion in upscaling lake methane emissions. We provide a first assessment of their prevalence across 4,572 lakes in four Arctic-boreal regions using airborne UAVSAR mapping and find that they cover 16.2 [13.9 – 19.1]% of Arctic-boreal lakes on average, a higher amount than other estimates, but with strong differences between study areas. Vegetated littoral zone areas (A_{VL}) are greatest in lowland riverine areas, where changing water levels cause seasonal variability. Consistent with previous studies, we find that littoral vegetation is more common in small than large lakes, but this relationship is weak and varies regionally. Accounting for A_{VL}, together with a synthesis of paired open water and littoral field measurements of methane flux, leads to an upscaling estimate 79 [68 - 94]% greater than an estimate that assigns the same pelagic flux to the entire lake. We conclude that remote sensing of littoral zones, based on vegetation or otherwise, and collection of flux data from both pelagic and littoral zones are necessary for accurate upscaling of lake methane emissions.

Acknowledgments

We thank Robert and Barbara Grandjambe for guiding services; Queenie Gray and Wood Buffalo National Park for enabling our field visits; Alex Shapiro of Alaska Land Exploration LLC for helicopter piloting; the U.S. Fish and Wildlife Service, the Gwichyaa Zhee Gwich'in Tribal Government and Doyon Limited for access to Yukon Flats National Wildlife Refuge; Michael W. Denbina for assistance with UAVSAR data processing; Kevin Timoney for assistance with botanical identifications; and Lawrence Vulis for a helpful review. Field work was conducted on or near land belonging to the Athabasca-Chipewyan, Mikisew Cree, Métis, and Gwich'in indigenous peoples. Resources supporting this work were provided by the NASA High-End Computing (HEC) Program through the NASA Center for Climate Simulation (NCCS) at Goddard Space Flight Center via the ABoVE Science Cloud. UAV Orthomosaics were created using DroneDeploy software. Data processing was made possible in part by the free and open-source software, including python, numpy, pandas, as well as with PolSAR Pro v5.1, which is provided by the European Space Agency (ESA). Any use of trade, firm, or product names is for descriptive purposes only and does not imply endorsement by the U.S. Government.

Funding

This work was funded by the following NASA programs; Future Investigators in NASA Earth and Space Science and Technology (FINESST), grant number 80NSSC19K1361, managed by Dr. Allison Leidner; Terrestrial Ecology Program Arctic-Boreal Vulnerability Experiment (ABoVE), grant number 80NSSC19M0104, managed by Dr. Hank Margolis; and the NASA Surface Water and Ocean Topography mission, grant number NNX16AH83G, managed by Dr. Nadya Vinogradova Shiffer. USGS LandCarbon Program provided funding for KPW, RGS, MMD, and FGT.

Data Availability

UAVSAR data used for this study can be downloaded at https://doi.org/10.5067/7PEQV8SVR4DM. The derivative land cover maps and lake vegetated littoral zone shapefiles can be found at the accompanying data publication: https://doi.org/10.3334/ORNLDAAC/1883. Methane flux data from the PAD can be downloaded at [EDI DOI to be updated]. All MATLAB and Python scripts used in data processing can be found at https://github.com/ekcomputer/random-wetlands and https://github.com/ekcomputer/PixelClassifier-fork [Zenodo DOI to be updated].

References

Ayoub, F., Jones, C. E., Lamb, M. P., Holt, B., Shaw, J. B., Mohrig, D., & Wagner, W. (2018). Inferring surface currents within submerged, vegetated deltaic islands and wetlands from multi-pass airborne SAR. *Remote Sensing of Environment*, *212*, 148–160.

https://doi.org/10.1016/j.rse.2018.04.035

Bansal, S., Johnson, O. F., Meier, J., & Zhu, X. (2020). Vegetation Affects Timing and Location of Wetland Methane Emissions. *Journal of Geophysical Research: Biogeosciences*, *125*(9), e2020JG005777. https://doi.org/10.1029/2020JG005777

Bastviken, D., Cole, J., Pace, M., & Tranvik, L. (2004). Methane emissions from lakes: Dependence of lake characteristics, two regional assessments, and a global estimate. *Global Biogeochemical Cycles*, *18*(4), 1–12. https://doi.org/10.1029/2004GB002238

Bastviken, D., Tranvik, L. J., Downing, J. A., Crill, P. M., & Enrich-Prast, A. (2011). Freshwater Methane Emissions Offset the Continental Carbon Sink. *Science*, *331*(6013), 50–50. https://doi.org/10.1126/SCIENCE.1196808

Bergström, I., Mäkelä, S., Kankaala, P., & Kortelainen, P. (2007). Methane efflux from littoral vegetation stands of southern boreal lakes: An upscaled regional estimate. *Atmospheric Environment*, *41*, 339–351. https://doi.org/10.1016/J.ATMOSENV.2006.08.014

Bourgeau-Chavez, L. L., Endres, S., Powell, R., Battaglia, M. J., Benscoter, B., Turetsky, M., … Banda, E. (2017). Mapping boreal peatland ecosystem types from multitemporal radar and optical satellite imagery. *Canadian Journal of Forest Research*, *47*(4), 545–559. https://doi.org/10.1139/cjfr-2016-0192

Bourgeau-Chavez, L. L., Graham, J. A., Endres, S., French, N. H. F., Battaglia, M., Hansen, D., & Tanzer, D. (2019). ABoVE: Ecosystem Map, Great Slave Lake Area, Northwest Territories, Canada, 1997-2011 (Version 1). ORNL Distributed Active Archive Center. https://doi.org/10.3334/ORNLDAAC/1695

Bridgham, S. D., Cadillo-Quiroz, H., Keller, J. K., & Zhuang, Q. (2013). Methane emissions from wetlands: biogeochemical, microbial, and modeling perspectives from local to global scales. *Global Change Biology*, *19*(5), 1325–1346. https://doi.org/10.1111/gcb.12131

Brown, J., Ferrians, O., Heginbottom, J. A., and Melnikov E. (2002). Circum-Arctic Map of Permafrost and Ground-Ice Conditions, Version 2 [Data set]. NSIDC. https://doi.org/10.7265/SKBG-KF16

Burger, M., Berger, S., Spangenberg, I., & Blodau, C. (2016). Summer fluxes of methane and carbon dioxide from a pond and floating mat in a continental Canadian peatland. *Biogeosciences*, *13*(12), 3777–3791. https://doi.org/10.5194/bg-13-3777-2016

Cheng, X., Huang, W., & Gong, J. (2014). Improved van Zyl polarimetric decomposition lessening the overestimation of volume scattering power. Remote Sensing, 6(7), 6365–6385. https://doi.org/10.3390/rs6076365

Parks Canada. (2019). *Wood Buffalo National Park World Heritage Site Action Plan* (Cat. No.: 978-0-660-27537-6). Retrieved from https://pcacdn.azureedge.net/-/media/pn-np/nt/woodbuffalo/2021-changes/02_11-action-plan-PDFs/WoodBuffalo-WHS-Action-Plan_EN.pdf

Casas-Ruiz, J. P., Jakobsson, J., & Giorgio, P. A. del. (2021). The role of lake morphometry in modulating surface water carbon concentrations in boreal lakes. *Environmental Research Letters*, *16*(7), 074037. https://doi.org/10.1088/1748-9326/AC0BE3

Casper, P., Maberly, S. C., Hall, G. H., & Finlay, B. J. (2000). Fluxes of methane and carbon dioxide from a small productive lake to the atmosphere. *Biogeochemistry*, *49*(1), 1–19. https://doi.org/10.1023/A:1006269900174

Christensen, T. R., Panikov, N., Mastepanov, M., Joabsson, A., Stewart, A., Öquist, M., … Svensson, B. (2003). Biotic controls on CO2 and CH4 exchange in wetlands – a closed environment study. *Biogeochemistry*, *64*(3), 337–354. https://doi.org/10.1023/A:1024913730848

Colmer, T. D. (2003). Long-distance transport of gases in plants: a perspective on internal aeration and radial oxygen loss from roots. Plant, Cell and Environment, 26(1), 17–36. https://doi.org/10.1046/j.1365-3040.2003.00846.x

Covey, K. R., & Megonigal, J. P. (2019). Methane production and emissions in trees and forests. *New Phytologist*, *222*(1), 35–51. https://doi.org/10.1111/NPH.15624

Dacey, J. W. H., & Klug, M. J. (1979). Methane efflux from lake sediments through water lilies. Science, 203(4386), 1253–1255. https://doi.org/10.1126/science.203.4386.1253

DelSontro, T., Beaulieu, J. J., & Downing, J. A. (2018). Greenhouse gas emissions from lakes and impoundments: Upscaling in the face of global change. *Limnology and Oceanography Letters*, *3*(3), 64–75. https://doi.org/10.1002/lol2.10073

DelSontro, T., Boutet, L., St-Pierre, A., del Giorgio, P. A., & Prairie, Y. T. (2016). Methane ebullition and diffusion from northern ponds and lakes regulated by the interaction between temperature and system productivity. *Limnology and Oceanography*, *61*(S1), S62–S77. https://doi.org/10.1002/lno.10335

DelSontro, T., del Giorgio, P. A., & Prairie, Y. T. (2018). No Longer a Paradox: The Interaction Between Physical Transport and Biological Processes Explains the Spatial Distribution of Surface Water Methane Within and Across Lakes. *Ecosystems*, *21*(6), 1073–1087. https://doi.org/10.1007/s10021-017-0205-1

Dove, A., Roulet, N., Crill, P., Chanton, J., & Bourbonniere, R. (1999). Methane dynamics of a northern boreal beaver pond. *Ecoscience*, *6*(4), 577–586.

Duarte, C. M., Kalff, J., Peters, R. H., & Peters, R. H. (1986). Patterns Biomass and Cover of Aquatic Macrophytes in Lakes. *Canadian Journal of Fisheries and Aquatic Sciences*, *43,* 1900–1908.

Engram, M., Walter Anthony, K. M., Sachs, T., Kohnert, K., Serafimovich, A., Grosse, G., & Meyer, F. J. (2020). Remote sensing northern lake methane ebullition. *Nature Climate Change*, *10(6)*, 511–517. https://doi.org/10.1038/s41558-020-0762-8

Freeman, A., & Durden, S. L. (1998). A three-component scattering model for polarimetric SAR data. *IEEE Transactions on Geoscience and Remote Sensing*. https://doi.org/10.1109/36.673687

Ghirardi, N., Bolpagni, R., Bresciani, M., Valerio, G., Pilotti, M., & Giardino, C. (2019). Spatiotemporal dynamics of submerged aquatic vegetation in a deep lake from sentinel-2 data. *Water*, *11*(3), 1–14. https://doi.org/10.3390/w11030563

Hastie, A., Lauerwald, R., Weyhenmeyer, G., Sobek, S., Verpoorter, C., & Regnier, P. (2018). CO2 evasion from boreal lakes: Revised estimate, drivers of spatial variability, and future projections. *Global Change Biology*, *24*(2), 711–728. https://doi.org/10.1111/GCB.13902

Hess, L. L., Melack, J. M., & Simonett, D. S. (1990). Radar detection of flooding beneath the canopy a review. *International Journal of Remote Sensing*, *11*(7), 1313–1325.

Holgerson, M. A., & Raymond, P. A. (2016). Large contribution to inland water CO2 and CH4 emissions from very small ponds. *Nature Geoscience*, *9*(3), 222–226. https://doi.org/10.1038/ngeo2654

Huttunen, J. T., Alm, J., Liikanen, A., Juutinen, S., Larmola, T., Hammar, T., … Martikainen, P. J. (2003). Fluxes of methane, carbon dioxide and nitrous oxide in boreal lakes and potential anthropogenic effects on the aquatic greenhouse gas emissions. *Chemosphere*, *52*, 609–621. https://doi.org/10.1016/S0045-6535(03)00243-1

Jensen, D., Cavanaugh, K. C., Simard, M., Christensen, A., Rovai, A., & Twilley, R. (2021). Aboveground biomass distributions and vegetation composition changes in Louisiana's Wax Lake Delta. *Estuarine, Coastal and Shelf Science*, *250*, 107139. https://doi.org/10.1016/j.ecss.2020.107139

Joabsson, A., Christensen, T. R., & Wallén, B. (1999). Vascular plant controls on methane emissions from northern peatforming wetlands. *Trends in Ecology & Evolution*, *14*(10), 385–388. https://doi.org/10.1016/S0169-5347(99)01649-3

Johnston, S. E., Striegl, R. G., Bogard, M. J., Dornblaser, M. M., Butman, D. E., Kellerman, A. M., … Spencer, R. G. M. (2020). Hydrologic connectivity determines dissolved organic matter biogeochemistry in northern high-latitude lakes. *Limnology and Oceanography Oceanography*. https://doi.org/10.1002/lno.11417

Juutinen, S., Alm, J., Larmola, T., Huttunen, J. T., Morero, M., Martikainen, P. J., & Silvola, J. (2003). Major implication of the littoral zone for methane release from boreal lakes. *Global Biogeochemical Cycles*, *17*(4). https://doi.org/10.1029/2003gb002105

Kankaala, P., Huotari, J., Tulonen, T., & Ojala, A. (2013). Lake-size dependent physical forcing drives carbon dioxide and methane effluxes from lakes in a boreal landscape. *Limnology and Oceanography*, *58*(6), 1915–1930. https://doi.org/10.4319/lo.2013.58.6.1915

Kankaala, P., Kaki, T., Makela, S., Ojala, A., Pajunen, H., & Arvola, L. (2005). Methane efflux in relation to plant biomass and sediment characteristics in stands of three common emergent macrophytes in boreal mesoeutrophic lakes. *Global Change Biology*, *11*(1), 145–153. https://doi.org/10.1111/j.1365-2486.2004.00888.x

Kyzivat, E. D., Smith, L. C., Pitcher, L. H., Arvesen, J., Pavelsky, T. M., Cooley, S. W., & Topp, S. (2018). ABoVE: AirSWOT Color-Infrared Imagery Over Alaska and Canada, 2018. ORNL Distributed Active Archive Center. https://doi.org/10.3334/ORNLDAAC/1643

Kyzivat, E. D., Smith, L. C., Pitcher, L. H., Fayne, J. V., Cooley, S. W., Cooper, M. G., … Pavelsky, T. M. (2019). A high-resolution airborne color-infrared camera water mask for the NASA ABoVE campaign. *Remote Sensing*, *11*, 1–28. https://doi.org/10.3390/rs11182163

Kyzivat, E. D., Smith, L. C., Pitcher, L. H., Fayne, J. V., Cooley, S. W., Cooper, M. G., Topp, S., Langhorst, T., Harlan, M. E., Gleason, C. J., & Pavelsky, T. M. (2020). ABoVE: AirSWOT Water Masks from Color-Infrared Imagery over Alaska and Canada, 2017 (Version 1). ORNL Distributed Active Archive Center. https://doi.org/10.3334/ORNLDAAC/1707

Kyzivat, E. D., Smith, L. C., Huang, C., Wang, C., Langhorst, T., Fayne, J. V., Harlan, M.E., Ishitsuka, Y., Feng, D., Dolan, W., Pitcher, L.H, Pavelsky, T. M. (2021). ABoVE: UAVSAR Lake and wetland classification for Yukon Flats, Peace-Athabasca Delta, and Canadian Shield, 2017-2019. ORNL Distributed Active Archive Center. https://doi.org/10.3334/ORNLDAAC/1883

Laanbroek, H. J. (2009). Methane emission from natural wetlands: interplay between emergent macrophytes and soil microbial processes. A mini-review.

Larmola, T., Alm, J., Juutinen, S., Huttunen, J. T., Martikainen, P. J., & Silvola, J. (2004). Contribution of vegetated littoral zone to winter fluxes of carbon dioxide and methane from boreal lakes. *J. Geophys. Res*, *109*. https://doi.org/10.1029/2004JD004875

Lehner, B., & Döll, P. (2004). Development and validation of a global database of lakes, reservoirs and wetlands. *Journal of Hydrology*, *296*, 1–22. https://doi.org/10.1016/j.jhydrol.2004.03.028

Li, M., Peng, C., Zhu, Q., Zhou, X., Yang, G., Song, X., & Zhang, K. (2020). The significant contribution of lake depth in regulating global lake diffusive methane emissions. *Water Research*, *172*, 115465. https://doi.org/10.1016/j.watres.2020.115465

Loken, L. C., Crawford, J. T., Schramm, P. J., Stadler, P., Desai, A. R., & Stanley, E. H. (2019). Large Spatial and Temporal Variability of Carbon Dioxide and Methane in a Eutrophic Lake. *Journal of Geophysical Research: Biogeosciences*, *124*(7), 2248–2266. https://doi.org/10.1029/2019JG005186

Mäkelä, S., Huitu, E., & Arvola, L. (2004). Spatial patterns in aquatic vegetation composition and environmental covariates along chains of lakes in the Kokemäenjoki watershed (S. Finland). *Aquatic Botany*, *80*(4), 253–269. https://doi.org/10.1016/j.aquabot.2004.08.006

Melton, J. R., Wania, R., Hodson, E. L., Poulter, B., Ringeval, B., Spahni, R., … Kaplan, J. O.

(2013). Present state of global wetland extent and wetland methane modelling: conclusions from a model inter-comparison project (WETCHIMP). *Biogeosciences*, *10*, 753–788. https://doi.org/10.5194/bg-10-753-2013

Meyer, M. F., Labou, S. G., Cramer, A. N., Brousil, M. R., & Luff, B. T. (2020). The global lake area, climate, and population dataset. Scientific Data 2020 7:1, 7(1), 1–12. https://doi.org/10.1038/s41597-020-0517-4

Michmerhuizen, C. M., Striegl, R. G., & McDonald, M. E. (1996). Potential methane emission from north-temperate lakes following ice melt. *Limnology and Oceanography*, *41*(5), 985–991. https://doi.org/10.4319/lo.1996.41.5.0985

Miller, C., Griffith, C. P., Goetz, S. J., Hoy, E. E., Pinto, N., McCubbin, I. B., … Margolis, H. A. (2019). An overview of ABoVE airborne campaign data acquisitions and science opportunities. *Environmental Research Letters*, *14*(8). https://doi.org/10.1088/1748-9326/ab0d44

NASA/JPL. (2017-2019). UAVSAR_POLSAR [Data set]. NASA Alaska Satellite Facility DAAC. https://doi.org/10.5067/7PEQV8SVR4DM

Natchimuthu, S., Sundgren, I., Gålfalk, M., Klemedtsson, L., Crill, P., Danielsson, Å., & Bastviken, D. (2016). Spatio-temporal variability of lake CH 4 fluxes and its influence on annual whole lake emission estimates. *Limnology and Oceanography, 61*(S1), S13–S26. https://doi.org/10.1002/lno.10222

Nelson, S. A. C., Cheruvelil, K. S., & Soranno, P. A. (2006). Satellite remote sensing of freshwater macrophytes and the influence of water clarity. *Aquatic Botany*, *85*(4), 289–298. https://doi.org/10.1016/j.aquabot.2006.06.003

Pavelsky, T. M., & Smith, L. C. (2008). Remote sensing of hydrologic recharge in the Peace-Athabasca Delta, Canada. *Geophysical Research Letters*. https://doi.org/10.1029/2008GL033268

Ribaudo, C., Bartoli, M., Longhi, D., Castaldi, S., Neubauer, S. C., & Viaroli, P. (2012). CO2 and CH4 fluxes across a Nuphar lutea (L.) Sm. stand. *Journal of Limnology*, *71*(1), 200–210.

Saunois, M., Stavert, A. R., Poulter, B., Bousquet, P., Canadell, J. G., Jackson, R. B., … Zhuang, Q. (2020). The Global Methane Budget 2000–2017. *Earth Syst. Sci. Data*, *12*, 1561–1623. https://doi.org/10.5194/essd-12-1561-2020

Schmiedeskamp, M., Stephanie, L., Praetzel, E., Bastviken, D., & Knorr, K.-H. (2021). Whole-lake methane emissions from two temperate shallow lakes with fluctuating water levels: Relevance of spatiotemporal patterns. *Limnol. Oceanogr*, *9999*, 1–15. https://doi.org/10.1002/lno.11764

Simard, M., Riel, B. V., Denbina, M., & Hensley, S. (2016). Radiometric Correction of Airborne Radar Images over Forested Terrain with Topography. *IEEE Transactions on Geoscience* *and Remote Sensing*, *54*(8), 4488–4500. https://doi.org/10.1109/TGRS.2016.2543142

Slaymaker, O. (2016). *Landscapes and Landforms of Western Canada*. Springer International Publishing.

Smith, L. K., & Lewis, W. M. (1992). Seasonality of methane emissions from five lakes and associated wetlands of the Colorado Rockies. *Global Biogeochemical Cycles*, *6*(4), 323–338. https://doi.org/10.1029/92GB02016

Smith, V. H., & Wallsten, M. (1986). Prediction of emergent and floating-leaved macrophyte cover in Central Swedish lakes. *Canadian Journal of Fisheries and Aquatic Sciences*, *43*(12), 2519–2523. https://doi.org/10.1139/f86-311

Spence, C., & Woo, M. (2006). Hydrology of subarctic Canadian Shield: heterogeneous headwater basins. *Journal of Hydrology*, *317*(1–2), 138–154. https://doi.org/10.1016/J.JHYDROL.2005.05.014

Stephanie, L., Praetzel, E., Plenter, N., Schilling, S., Schmiedeskamp, M., Broll, G., … Praetzel@uni-Muenster, L. De. (2020). Organic matter and sediment properties determine in-lake variability of sediment CO 2 and CH 4 production and emissions of a small and shallow lake. *Biogeosciences*, *17*, 5057–5078. https://doi.org/10.5194/bg-17-5057-2020

Striegl, R. G., Dornblaser, M. M., McDonald, C. P., Rover, J. R., & Stets, E. G. (2012). Carbon dioxide and methane emissions from the Yukon River system. *Global Biogeochemical Cycles*, *26*(4). https://doi.org/10.1029/2012GB004306

Striegl, R. G., & Michmerhuizen, C. M. (1998). Hydrologic influence on methane and carbon dioxide dynamics at two north-central Minnesota lakes. *Limnology and Oceanography*, *43*(7), 1519–1529. https://doi.org/10.4319/lo.1998.43.7.1519

Ström, L., Mastepanov, M., & Christensen, T. R. (2005). Species-specific Effects of Vascular Plants on Carbon Turnover and Methane Emissions from Wetlands. *Biogeochemistry*, *75*(1), 65–82. https://doi.org/10.1007/s10533-004-6124-1

Thornton, B. F., Wik, M., & Crill, P. M. (2016). Double-counting challenges the accuracy of high-latitude methane inventories. *Geophysical Research Letters*, *43*(24), 12,569-12,577. https://doi.org/10.1002/2016GL071772

Timoney, K. P. (2013). *The Peace-Athabasca Delta: Portrait of a Dynamic Ecosystem*. Edmonton: University of Alberta Press.

Töyrä, J., & Pietroniro, A. (2005). Towards operational monitoring of a northern wetland using geomatics-based techniques. Remote Sensing of Environment, 97(2), 174–191. https://doi.org/10.1016/J.RSE.2005.03.012

Tranvik, L. J., Downing, J. A., Cotner, J. B., Loiselle, S. A., Striegl, R. G., Ballatore, T. J., … Weyhenmeyer, G. A. (2009). Lakes and reservoirs as regulators of carbon cycling and climate. *Limnology and Oceanography*, *54*(6part2), 2298–2314.

https://doi.org/10.4319/lo.2009.54.6_part_2.2298

Ulander, L. M. H. (1996). Radiometrie slope correction of synthetic-aperture radar images. *IEEE Transactions on Geoscience and Remote Sensing*, *34*(5), 1115–1122. https://doi.org/10.1109/36.536527

Verpoorter, C., Kutser, T., Seekell, D. A., & Tranvik, L. J. (2014). A global inventory of lakes based on high-resolution satellite imagery. *Geophysical Research Letters*, *41*(18), 6396–6402. https://doi.org/10.1002/2014GL060641

Villa, J. A., Ju, Y., Yazbeck, T., Waldo, S., Wrighton, K. C., & Bohrer, G. (2021). Ebullition dominates methane fluxes from the water surface across different ecohydrological patches in a temperate freshwater marsh at the end of the growing season. *Science of the Total Environment*, *767*, 144498. https://doi.org/10.1016/j.scitotenv.2020.144498

Wang, J. A., Sulla-menashe, D., Woodcock, C. E., Sonnentag, O., Keeling, R. F., & Friedl, M. A. (2019). ABoVE: Landsat-derived Annual Dominant Land Cover Across ABoVE Core Domain, 1984-2014. ORNL Distributed Active Archive Center. https://doi.org/10.3334/ORNLDAAC/1691

Wang, J. A., Sulla-Menashe, D., Woodcock, C. E., Sonnentag, O., Keeling, R. F., & Friedl, M. A. (2019). Extensive land cover change across Arctic–Boreal Northwestern North America from disturbance and climate forcing. *Global Change Biology, 00*, 1–16. https://doi.org/10.1111/gcb.14804

Ward, E. M., & Gorelick, S. M. (2018). Drying drives decline in muskrat population in the Peace-Athabasca Delta, Canada. *Environmental Research Letters*, 13, 124026. https://doi.org/10.1088/1748-9326/aaf0ec

West, W. E., Creamer, K. P., & Jones, S. E. (2016). Productivity and depth regulate lake contributions to atmospheric methane. Limnology and Oceanography, 61(S1), S51–S61. https://doi.org/10.1002/LNO.10247

Wetzel, R. G. (1990). Land-water interfaces: Metabolic and limnological regulators. *Verh. Internat. Verein. Limnol.*, *24*(September), 6–24.

Wetzel, R. G. (2001). *Limnology: Lake and River Ecosystems* (Third). Boston: Academic Press.

Wik, M., Varner, R. K., Anthony, K. W., MacIntyre, S., & Bastviken, D. (2016). Climate-sensitive northern lakes and ponds are critical components of methane release. *Nature Geoscience*, *9*(2), 99–105. https://doi.org/10.1038/ngeo2578

Wolfe, B. B., Hall, R. I., Last, W. M., Edwards, T. W. D., English, M. C., Karst-Riddoch, T. L., … Palmini, R. (2006). Reconstruction of multi-century flood histories from oxbow lake sediments, Peace-Athabasca Delta, Canada. Hydrological Processes, 20(19), 4131–4153. https://doi.org/10.1002/hyp.6423

Zhang, B., Tian, H., Lu, C., Chen, G., Pan, S., Anderson, C., & Poulter, B. (2017). Methane emissions from global wetlands: An assessment of the uncertainty associated with various wetland extent data sets. *Atmospheric Environment*, *165*, 310–321. https://doi.org/10.1016/J.ATMOSENV.2017.07.001

Zhang, S., Foerster, S., Medeiros, P., de Araújo, J. C., & Waske, B. (2018). Effective water surface mapping in macrophyte-covered reservoirs in NE Brazil based on TerraSAR-X time series. *International Journal of Applied Earth Observation and Geoinformation, 69*, 41–55. https://doi.org/10.1016/j.jag.2018.02.014

Zhang, Y., Jeppesen, E., Liu, X., Qin, B., Shi, K., Zhou, Y., … Deng, J. (2017). Global loss of aquatic vegetation in lakes. *Earth-Science Reviews*, *173*, 259–265. https://doi.org/https://doi.org/10.1016/j.earscirev.2017.08.013

Zhang, Z., Ni, W., Sun, G., Huang, W., Ranson, K. J., Cook, B. D., & Guo, Z. (2017). Biomass retrieval from L-band polarimetric UAVSAR backscatter and PRISM stereo imagery. *Remote Sensing of Environment*, *194*, 331–346. https://doi.org/10.1016/J.RSE.2017.03.034

Zhang, Z., Fluet-Chouinard, E., Jensen, K., Mcdonald, K., Hugelius, G., Gumbricht, T., … Poulter, B. (2021). Development of the global dataset of Wetland Area and Dynamics for Methane Modeling (WAD2M). Earth Syst. Sci. Data, 13. https://doi.org/10.5194/essd-13-2001-2021